CHAPTER 19

Imaging Modalities for Manganese Toxicity

ULRIKE DYDAK*[a,b] AND SUSAN R. CRISWELL[c,d]

[a] School of Health Sciences, Purdue University, 550 Stadium Mall Drive, West Lafayette, Indiana 47907, USA; [b] Department of Radiology and Imaging Sciences, Indiana University School of Medicine, Indianapolis, Indiana, USA; [c] Department of Neurology, Washington University School of Medicine, St. Louis, Missouri, USA; [d] American Parkinson Disease Association Advanced Center for Parkinson Research, St. Louis, Missouri, USA
*Email: udydak@purdue.edu

19.1 Introduction

Over the past decades, the novel possibilities and available technology of *in vivo* imaging have significantly advanced the field of neuroscience, and in particular they have contributed to the study of manganese (Mn) neurotoxicity. This chapter describes several of the imaging modalities that have made an impact in Mn neurotoxicity research. Some of these imaging modalities are targeted at measuring the body burden of Mn, either indirectly as with magnetic resonance imaging (MRI), or directly with X-ray fluorescence imaging. Others are imaging morphological and biochemical changes due to Mn exposure using positron emission tomography (PET), single photon emission computed tomography (SPECT), magnetic resonance (MR) volumetry, MR diffusion weighted imaging or MR spectroscopy, thereby measuring the effect of Mn exposure.

Issues in Toxicology No. 22
Manganese in Health and Disease
Edited by Lucio G. Costa and Michael Aschner

Published by the Royal Society of Chemistry, www.rsc.org

For each modality, the basic principle of the imaging technique will be briefly described to facilitate proper interpretation and understanding of the limitations with regard to imaging Mn neurotoxicity. This will be followed by a discussion of the main findings using that modality, and how they have shaped our understanding of Mn neurotoxicity.

19.2 Magnetic Resonance Imaging

19.2.1 Basics of MRI

MRI is a non-invasive medical imaging technique that enables the *in vivo* study of tissue, with high ($\sim$1 mm) resolution and good soft tissue contrast. It also provides a variety of functional assessments, such as the measurement of blood oxygenation, blood flow, metabolism, and diffusion properties. MRI makes use of the nuclear magnetic properties of hydrogen nuclei (protons), which possess an intrinsic angular momentum (spin). Given that living tissue contains a large fraction of water, the MRI signal stems primarily from the hydrogen nuclei in water molecules. Placed into an external magnetic field, the proton spins will align either with or against the magnetic field and precess about the field at a specific frequency called the Larmor frequency. The Larmor frequency depends both on the type of nucleus (in MRI mostly hydrogen) and on the strength of the magnetic field at the location of the nucleus. By irradiating the tissue with electromagnetic radiation at this particular Larmor frequency, a resonance effect can be obtained. Absorption of the radiation results in ''flipping'' the spins into the higher energy state, also called excitation of the spins. When the irradiation stops, the spins stochastically flip back to their ground state, emitting an exponentially decaying electromagnetic signal of the same frequency – the MRI signal. At clinical magnetic field strengths of MRI scanners, 1.5 and 3 tesla (T), the resonance frequency lies in the radiofrequency (RF) domain and is thus considered harmless to the human body.

The image contrast of different tissue types results from the different decay constants of the emitted MRI signal, which are also called relaxation times. Relaxation can be achieved through two different mechanisms, which occur simultaneously but at different rates. A spin can shed excessive energy by interaction between the spin and its atomic environment, causing it to return to its longitudinal alignment parallel to the magnetic field. The time associated with this relaxation mechanism is the spin–lattice relaxation time, $T1$. Another way for the observed signal to decay is through random spin–spin interaction, which causes the coherently precessing individual spins to dephase, thereby cancelling out their sum. The associated relaxation time is termed the spin–spin relaxation time, $T2$. External field inhomogeneities, introduced by tissue type variations, blood flow, or even air in the tissue to be imaged, cause an even faster dephasing and thus signal decay, characterized by the $T2^*$ relaxation time. In general the image intensity (contrast) of a particular tissue depends on its proton density, and on its

relaxation times, $T1$, $T2$ and $T2^*$. By varying several imaging parameters, in particular the timing between repeated RF excitations, or between excitation and recording of the signal, the image contrast can be changed to depend mostly on the $T1$ relaxation time ($T1$-weighted imaging), or mostly on the $T2$ relaxation time ($T2$-weighted imaging).

19.2.2 Manganese as MRI Contrast Agent

Manganese, in the form of Mn^{2+}, is strongly paramagnetic and thus highly influences the relaxation properties of neighboring protons. It is important to note that MRI images depicting Mn deposition in tissue do so not by directly imaging the Mn nuclei, but they instead reflect its role as a contrast agent. The presence of Mn changes the magnetic relaxation properties of the hydrogen nuclei that are imaged (Figure 19.1).

As a paramagnetic contrast agent, Mn shortens both the $T1$ and the $T2$ relaxation times of the protons in water molecules.[1–6] Tissue with short $T1$ will appear bright in $T1$-weighted imaging, and thus Mn accumulation in the brain results in higher signal intensity in $T1$-weighted images (positive contrast). In $T2$-weighted images, tissue with longer $T2$ will contribute more

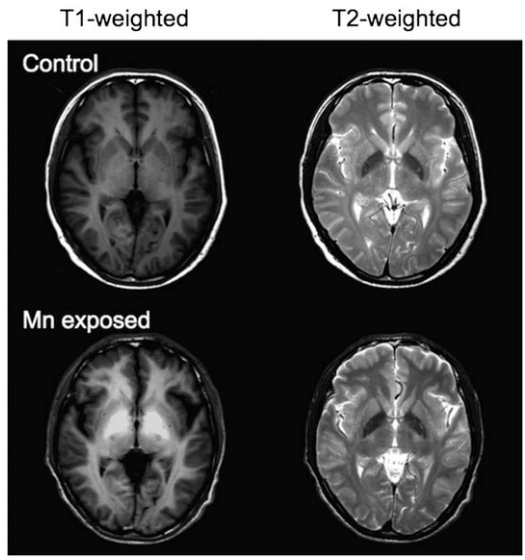

Figure 19.1 $T1$-weighted (left) and $T2$-weighted (right) MRI images of the same brain slice in an unexposed control subject (top row) and a Mn-exposed metal worker (bottom row). The bright signal in the globus pallidus and surrounding areas in the $T1$-weighted image of the exposed subject reflects increased Mn concentration. The dark signal intensity of the globus pallidus in the $T2$-weighted images reflects the effects of a large iron content in the globus pallidus (seen in both subjects) as well as the increased Mn deposition (a combined effect in the exposed subject).

to the signal and appear brighter. By shortening *T*2, Mn decreases the signal intensity in *T*2-weighted images (negative contrast). However, *T*1-weighted imaging is used more commonly to detect Mn deposition, because for most tissues *T*1-weighted imaging is somewhat more sensitive than *T*2-weighted imaging.

The relaxation times depend on other properties besides the Mn concentration alone, such as the molecular configuration in which Mn resides.[2] In addition, other paramagnetic metals, such as iron, have similar effects on MRI relaxation properties. The combined influence with Mn on MRI signal contrast is complicated, especially because Mn and iron (Fe) concentrations are not fully independent of each other in physiological systems. A model for the analysis of competitive relaxation effects of Mn and Fe *in vivo* is presented in Zhang *et al.*[7] Absolute quantification of manganese by means of MRI is therefore anything but straightforward.

19.2.2.1 T*1-Weighted MRI in Mn Toxicity Studies*

Newland *et al.* were among the first to use MRI to assess Mn deposition in a toxicity study in non-human primates,[8] reporting Mn uptake in the caudate nucleus, lenticular nuclei, substantia nigra, pituitary gland and a region corresponding to the subthalamic nucleus and ventromedial hypothalamus. Since then, a wealth of human studies have shown that increased Mn exposure can result in significant signal changes in *T*1-weighted images of Mn-exposed workers.[9–21] Similar hyperintensities are found in patients with reduced hepatobiliary excretion of Mn,[22–34] in patients receiving total parenteral nutrition (TPN),[35–41] as well as in subjects addicted to the drug methcathinone (ephedrone).[42–49]

In non-human primates, as well as in humans, Mn-induced signal changes are highest in the globus pallidus, adjacent basal ganglia regions, and the pituitary gland (see Figure 19.2), intermediate in the caudate and putamen, and lowest in other gray matter and white matter regions. However, many brain structures have by now been shown to exhibit *T*1-weighted hyperintensities, or a reduction in measured *T*1 relaxation times after Mn exposure, including the medial cerebral peduncle[50] and the olfactory bulb.[21] Moreover, quantitative evaluation of the signal intensities shows that white matter areas also accumulate Mn.[21,51,52]

In contrast to human and non-human primates, Mn-induced *T*1 hyperintensities in rodents first appear in the choroid plexus and ventricles,[53] and subsequently in the pituitary gland, olfactory bulb and cortical regions such as the hippocampus.[50,54]

*T*1-weighted MRI can also be used to monitor the efficacy of treatment or to assess the effect of cessation of Mn exposure. For example, in one report, chelation therapy resulted in a reversal of the *T*1 signal increase,[55] while other studies have reported vanishing hyperintensities within approximately six months after workers were no longer exposed in an occupational setting.[14,18] In contrast, the average half-life of Mn in the rat brain has been reported as

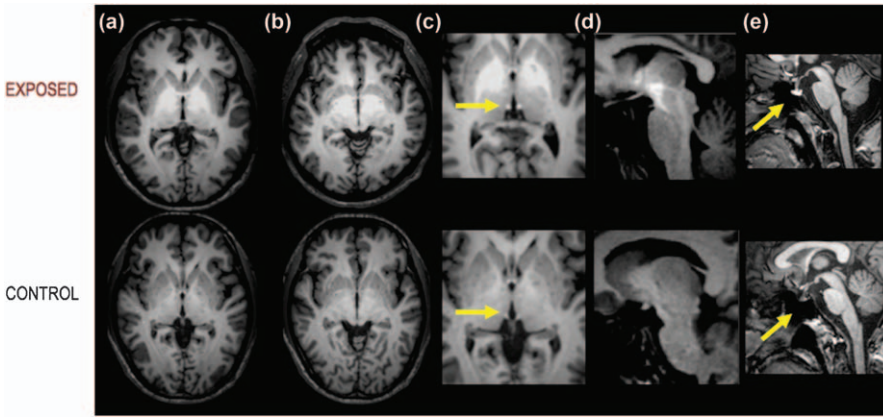

Figure 19.2 *T*1-weighted MRI images from a Mn-exposed smelter (top row) and a non-exposed control subject, showing hyperintensities in (a) the globus pallidus and part of the thalamus, (b) subthalamic nucleus, (c) pineal stalk, (d) medial cerebral peduncle and (e) pituitary gland.[50] (Reproduced with permission from Dydak *et al*., *Proc. Intl. Soc. Mag. Reson. Med*., 2011, **19**, 1428).

51–74 days.[56] In non-human primates the elimination rate is suggested to be brain region specific, with an average half-life ranging from 33 days[57] to 53 days[58] after inhalational and subcutaneous Mn exposure, respectively.

19.2.2.2 The Pallidal Index

The pallidal index (PI) is a popular approach to quantifying the hyperintensities in *T*1-weighted MRI images that correspond to increased Mn concentrations. First introduced by Krieger *et al*. in 1995,[27] the PI reflects the relative signal intensity in a *T*1-weighted image of the globus pallidus *vs*. the adjacent subcortical frontal white matter. This measure is relatively easy to obtain from MRI data, usually by placing a region of interest (ROI) in the globus pallidus and one in frontal white matter (Figure 19.3), then taking the ratio of the mean signal intensities of each ROI and multiplying by 100.

$$\mathrm{PI} = \frac{\mathrm{Signal}_{\mathrm{Global\ Pallidus}}}{\mathrm{Signal}_{\mathrm{Frontal\ WM}}} \times 100 \qquad (19.1)$$

The PI has been used in many MRI studies on Mn neurotoxicity, both in animal models and in humans. In rats, significant correlations between the concentration of Mn in the globus pallidus, as measured by *ex vivo* techniques, and the PI measured by MRI were reported as early as 2001.[59] In 2006 Dorman *et al.*[52] presented the first comprehensive study comparing the PI, the relaxation rate $R1$ ($=1/T1$), and a histological analysis of brain Mn concentrations. This paper established linear relationships between the PI in rhesus monkeys and manganese concentrations in both the globus pallidus and in whole blood. They also reported linear relationships between the $R1$

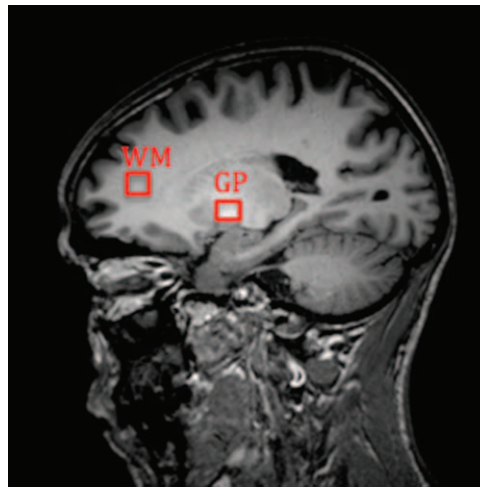

Figure 19.3 Sagittal image of a Mn-exposed worker, showing placement of ROIs in the globus pallidus and in frontal white matter for the calculation of the pallidal index.
(Reproduced with permission from Dydak *et al.*, *Environmental Health Perspectives*, 2011, **119**, 219–224).

relaxation rate and white matter Mn, pituitary Mn and globus pallidus Mn concentrations. Finding a decrease in *T*1 in white matter as well, Dorman *et al.* were the first to note that the PI may be less sensitive than direct measurement of *T*1 relaxation, because the calculation of the PI assumes that white matter is unaffected. For this reason Guilarte *et al.*[51] suggested using a ''PI equivalent'', using signal from pericranial muscle – which is not assumed to take up any Mn – as the reference region, and expanding the idea of the PI to many other brain regions in addition to the globus pallidus. Using the ''PI equivalent'', this group found higher signal intensity ratios in Mn-exposed non-human primates, not only for the globus pallidus, but also for the pituitary gland, caudate, putamen and substantia nigra.[51] Their findings confirmed that the *T*1-weighted signal in white matter also increases during Mn administration.

Early human studies already suggested that an increase in PI could document increases in brain Mn levels prior to the onset of clinical symptoms of manganism, showing correlations between the PI and blood Mn levels[15] and cumulative exposure.[10] These dependencies were confirmed in an imaging study on 111 Mn exposed workers (welders, smelters and welding rod manufacturers) conducted by Kim *et al.*,[60] whose regression model reveals significant contributions of both airborne and blood manganese to the PI. They further describe a correlation between the PI and decreased performance on neurological tests. Another study looking at neurobehavioral performance also found the PI to be a predictor for several neurobehavioral test scores such as the digit symbol, digit span backward, Stroop word, Stroop error index, and grooved pegboard scores.[61]

19.2.2.3 Relaxometry to Quantify Brain Mn

The exact value of the pallidal index is dependent on image parameters, such as resolution, slice thickness, and contrast; on the choice and reproducibility of the ROI used to calculate the signal intensity; and finally on the assumption that the reference region is not affected by Mn. A multitude of studies have compared the PI to the direct measurement of the physical MR property of *T*1 relaxation. The value of *T*1 (or the relaxation rate *R*1) is dependent on the main magnetic field strength (*e.g.* using a 1.5 T or 3 T scanner), but should be fully user independent. The MRI sequences necessary for this measurement are more complex and take longer than the scans that yield the PI, and they require sophisticated calculations to extract the *T*1 value. Nonetheless, most clinical MRI scanners today offer the necessary sequences and postprocessing tools.

Early animal studies established correlations between relaxation rates and tissue Mn concentrations.[59,62] In 2006 Dorman *et al.* pointed out that the direct measurement of the *R*1 rate is more exact than using the PI,[52] as noted above. In 2007, Choi *et al.* found in human MRI studies that the blood Mn level correlated only with the *T*1 relaxation time, but not with the PI, and that the *T*1 correlation with PI was only present at higher levels of the PI.[63] Similarly, Sen *et al.* reported group differences in *T*1 relaxation times and normalized *T*1w signal intensities (not using a ratio) in several brain regions between welders and non-exposed workers in the US, yet saw no differences in the PI.[21] Moreover, they found no correlations of the PI with fine motor measures, yet these correlations were present for the normalized signal intensities. While the PI may prove robust for higher Mn exposures that lead to clearly visible *T*1 hyperintensities in MRI images, as were observed for example in many of the early human studies, it appears that measurement of the *T*1 relaxation time is more reliable at the lower exposure settings found in newer studies, where hyperintensities are seldom seen with the naked eye due to recent regulatory limitations on Mn exposure in work settings.

Measurement of *T*2 and *T*2* in the substantia nigra as a means of assessing the iron concentration in this brain area has been suggested to provide a good marker of disease progression in Parkinson disease.[64] Yet to date only one study has looked at *T*2* in Mn exposed workers: Long *et al.* reported reduced *T*2* levels in the frontal cortex in welders, another indication for the involvement of the frontal cortex in Mn neurotoxicity.[16] Whether such a reduction of *T*2* is caused by iron deposition as a side effect of Mn exposure, or as direct effect of Mn deposition, or as a combination of both, is subject of ongoing research.

19.2.2.4 MEMRI – Mn-Enhanced MRI

In parallel to the first use of MRI to study Mn accumulation in the brains of exposed animals and humans, the research field of Mn-enhanced MRI (MEMRI) has evolved. In MEMRI, a technique first described in 1998, an

injection of Mn^{2+} is used as a powerful MRI contrast agent. MEMRI has revolutionized the field of neuroscience by enabling the *in vivo* tracing of neuronal connections, monitoring neuronal activity and visualizing axonal regeneration.[65] Extensive reviews on the field of MEMRI research can be found by Silva,[66] Koretsky[67] and Inoue,[65] describing three main groups of applications. The first is neuronal tract tracing *in vivo*, first described by Pautler *et al.*,[68] which makes use of the fact that Mn^{2+} enters neurons *via* voltage gated calcium (Ca^{2+}) channels, gets released at the synapse, and is then taken up by postsynaptic neurons. This property enables MRI-detectable *in vivo* trans-synaptic tract tracing, with the paramagnetic Mn^{2+} ion providing localized enhancement of $T1$ relaxation. The second group of applications uses activity-induced Mn-enhanced MRI (AIM-MRI) as a functional MRI technique to monitor neuronal activity.[69] Given that Mn^{2+} serves as an analog for Ca^{2+}, increases in Ca^{2+} influx in response to increased neuronal activity lead to increased local concentrations of Mn^{2+} and thus can be monitored by MRI.[70] The third group of applications uses Mn^{2+} as a contrast agent to enhance anatomical detail in the visualization of neural architecture.[71,72]

Owing to the cellular toxicity of larger concentrations of Mn^{2+}, MEMRI remains confined to research in animal models, where it has been successfully applied to study small amphibians, such as frogs, as well as songbirds, rodents, and non-human primates. Since MEMRI is based on single injections of high concentrations of Mn^{2+} (up to 180 mg kg^{-1} in rodents with systemic administration), it does not serve the purpose of studying the effects of *chronic* exposure to Mn, as is of interest in environmental and occupational health sciences. However, the very same characteristics of Mn applied in MEMRI are also useful for the study of Mn deposition in the brain due to chronic, low-concentration Mn exposure, both in animals and in humans. For example MEMRI studies confirm that temporal changes of the relaxation times $T1$ and $T2$, measured in the olfactory bulb and cortex for 35 days after systemic administration of Mn, are inversely proportional to the underlying tissue Mn concentration and reflect the total amount of Mn present in the tissue.[73] The same authors also used MEMRI to detect Mn^{2+} transport from the rat olfactory bulb through appropriate brain structures to the amygdala in individual animals.[74]

In recent years, researchers using MEMRI have become more alert to the toxic effects of Mn to the brain and therefore the number of MEMRI studies investigating these toxic effects is increasing. Several MEMRI studies have looked into ways to reduce the toxicity and increase tolerance to MEMRI by studying small-dose ($\sim$30 mg kg^{-1} $MnCl_2$) fractionated injection schemes,[75] the biological half-life of Mn,[56] and the spatial distribution and time course of Mn uptake and washout in different animal models (Figure 19.4).[66] These studies in turn are of high interest for the interpretation of Mn-induced MRI signal hyperintensities in human studies with chronic exposure settings.

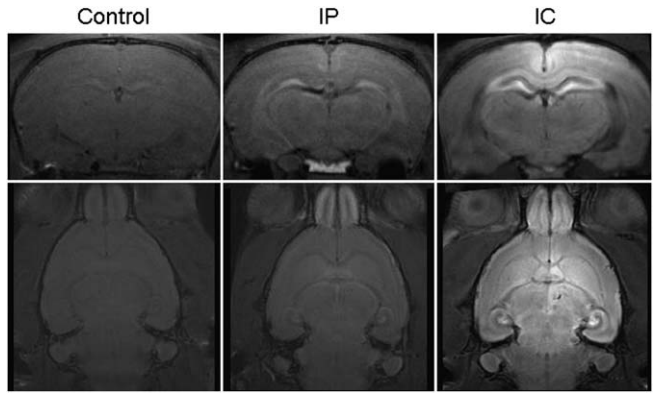

Figure 19.4 MEMRI images. Coronal (top) and axial (bottom) MEMRI images of rat hippocampus 24 h after Mn injection: control, intraperitoneal (IP) injection ($MnCl_2$, 30 mg kg^{-1}) and intracerebral (IC) injection ($MnCl_2$, 10 μl, 50 mM). Increased Mn accumulation in the hippocampus is clearly visible following both types of injection, with the IC injection of Mn resulting in increased contrast.
(Reprinted from NeuroImage 64, A. Daoust, E. L. Barbier, S. Bohic, Manganese enhanced MRI in rat hippocampus: A correlative study with synchrotron X-ray microprobe, Pages 10–18, Copyright 2013, with permission from Elsevier.)

19.2.3 Morphological Changes Assessed by MRI

In addition to the indirect measure of tissue Mn enabled by the Mn-induced contrast change in MRI images, MRI offers a variety of morphological and functional measures of physiological states. Amongst these are changes in brain region volumes (atrophy) as measured by MR volumetry, changes in metabolism as measured by magnetic resonance spectroscopy (MRS), changes in tissue diffusion properties as measured by diffusion weighted imaging (DWI), and changes in functional activity of particular brain areas as measured by functional MRI (fMRI). While these measures are not specific to Mn neurotoxicity, they have been used extensively to assess functional outcomes or to search for biomarkers of Mn neurotoxicity. These MRI methods and their findings relevant to Mn neurotoxicity are briefly discussed in the following subsections.

MR volumetry techniques, which include voxel-based morphometry (VBM), use whole-brain high resolution MRI images (usually *T*1-weighted) with good contrast between gray and white matter. The image dataset is segmented into different types of brain matter (white matter, gray matter and cerebrospinal fluid), as well as into individual brain areas. This enables the determination of total brain volume as well as volumes of individual brain regions. According to its contrast, each image pixel gets assigned a probability of belonging to gray matter, white matter or cerebrospinal fluid. In addition each pixel may also be attributed to a particular brain region, *e.g.*

the hippocampus, with a certain probability. Adding the probabilities of belonging to gray matter over all pixels within a particular brain region gives a measure of ''gray matter density'' for the respective brain region. Usually images are normalized to a brain atlas and undergo several smoothing and filtering steps, which then allows for the assessment of group differences in brain volumes from particular brain areas between exposed and non-exposed individuals.

While currently ongoing research is making more and more use of MR volumetry, relatively few reports of volume changes associated with Mn exposure are found in the literature. In 2011 a MEMRI study investigated long-term consequences of using Mn as contrast agent in rats. Comparing animals studied with MEMRI, *i.e.* with Mn administered on a regular basis, to animals receiving MRI scans without contrast agents over a period of six months, the authors found that the MEMRI animals showed progressive signs of cerebral toxicity, including progressive brain volume decrease as measured by MR volumetry.[76] Atrophy was observed in whole brain volume differences, as well as in regional differences between MEMRI animals and untreated animals in amygdala, hippocampus, thalamus and cortex. In Mn-exposed welders, Chang *et al.* found significantly diminished brain volumes in the globus pallidus and cerebellar regions that were associated with cognitive and fine motor performance.[77] In combination with the hyper-intensities seen in Mn-exposed workers, this measure may indicate subtle structural abnormalities in the exposed group.

A potential confounder of this method is the fact that image contrast is used to classify the tissue type of each pixel – yet Mn accumulation affects the contrast by changing the relaxation times. This may result in incorrect tissue classifications and thus wrongly calculated volumes. For example, the obvious hyperintensity in the *T*1-weighted image of the Mn-exposed worker displayed in Figure 19.1 clearly does not allow for correct segmentation of the globus pallidus using those images. In more subtle cases of Mn accumulation, thorough testing of the segmentation algorithm is necessary before volumetric results may be interpreted.

19.2.4 Magnetic Resonance Spectroscopy

Magnetic resonance spectroscopy (MRS) is based on the same physical principles as MRI. It complements MRI by providing biochemical information based on the chemical shift effect: the same nuclei can absorb and emit electromagnetic energy at slightly different resonance frequencies depending on their chemical environment in molecules. Thanks to this frequency separation (expressed as a chemical shift difference), concentrations of different metabolites and chemical compounds can be measured in living tissue. MRS can be used with a variety of nuclei, but the proton (^{1}H) is the most common choice *in vivo*, owing to its abundance in the human body, its high intrinsic sensitivity, and the fact that MR scanner hardware is tuned by default for protons.

A typical short-echo-time ^{1}H spectrum acquired from a human brain region at 3 T features a number of important metabolites, such as *N*-acetyl aspartate (NAA, a marker for neuronal integrity), total creatine (tCr, an energy buffer and energy shuttle), choline (Cho, involved in phospholipid synthesis and degradation), myo-inositol (mI, a glial cell marker), the main excitatory neurotransmitter glutamate (Glu), and the closely related compound glutamine (Gln) (Figure 19.5). Since the MRS signals of Glu and Gln are hard to differentiate at lower field strength, the sum of Glu and Gln, known as Glx, is often reported. The spectrum also contains macromolecules and lipids, which give rise to the broad baseline underneath the prominent peaks. A variety of other neurochemical compounds, such as the main inhibitory neurotransmitter gamma aminobutyric acid (GABA) and the antioxidant glutathione (GSH), also contribute to a ^{1}H MRS spectrum, but cannot readily be measured by acquiring a standard brain spectroscopy scan at clinical magnetic field strengths. This inability is due to the low *in vivo* concentration of these compounds and the fact that their resonances are concealed by much larger peaks of other brain metabolites. To detect them, an indirect intramolecular spin–spin interaction known as J-coupling (which splits peaks into multiplets) can be exploited to select species of interest while cancelling out unwanted signal. In particular, J-difference editing

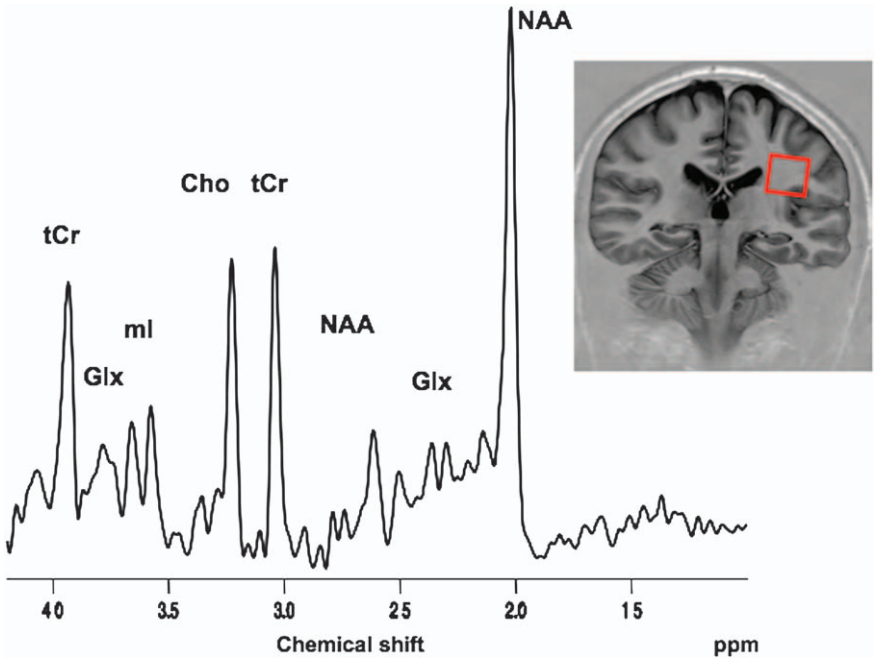

Figure 19.5 Typical spectrum acquired in parietal white matter of a human brain at 3 T, showing the signal peaks of *N*-acetyl aspartate (NAA), Glx (=Glutamate + Glutamine), total creatine (tCr), choline-containing compounds (Cho) and myo-inositol (mI).

using point resolved spectroscopy with Mescher–Garwood (MEGA) suppression (MEGA-PRESS) is a commonly used sequence for spectral editing of GABA,[78–80] revealing a GABA resonance at a chemical shift of 3.0 ppm. *In vivo* dopamine cannot be measured by MRS owing to its very low concentration, but it can be assessed by PET and SPECT as discussed later in this chapter. The higher field strength (typically 7–14 T) and better magnetic field homogeneity of animal MR scanners or nuclear magnetic resonance (NMR) spectrometers allow for quantification and identification of several additional brain metabolites in rodent brains or tissue extracts. The resulting full set of MRS-derived metabolite information is often called the neurochemical profile.[81]

The ability of MRS to make an early, non-invasive diagnosis is highly valued by clinicians, and MRS is increasingly incorporated into clinical protocols for brain examinations in selected patients.[82] However, the lack of standardized protocols, analysis techniques and reporting of results has led in many cases to a wide range of reported changes for the same disorder. Nevertheless, it is generally accepted that the characteristic MRS feature of neurodegenerative diseases such as Alzheimer disease and Parkinson disease is primarily a decrease in total NAA, reflecting the degeneration of the neurons. In addition, decreased Glu levels, an elevated Cho level and elevated mI levels have been associated with neurodegeneration in various studies.[82]

To study the mechanism of manganese neurotoxicity, MRS has been used to obtain metabolic information from Mn-exposed cell cultures and animal models, as well as occupationally exposed human workers. In an MRS study of Mn-treated cultured cells, Glu was found to decrease in neurons and neuron–astrocyte co-cultures, and decreases in mI were also observed in the co-cultures.[83] A high resolution NMR spectroscopy study on tissue extracts found a selective decrease of NAA in the globus pallidus of rats after Mn exposure, as well as decreased Gln, Cho and Glu, which was paralleled by accumulation of GABA.[84] Decreased NAA and Glu levels were reported in the hypothalamus of overnight food-suppressed rats after Mn dosing.[85] Furthermore, Guilarte *et al.* found a significant decrease of NAA in the parietal cortex of Mn-exposed non-human primates,[51] indicating decreased neuronal integrity in these Mn-treated animal models.

In humans, Kim *et al.*[86] studied the basal ganglia of welders using MRS, but did not see any significant changes in NAA : Cr, Cho : Cr and NAA : Cho ratios. Chang *et al.*[87] investigated frontal gray matter and parietal white matter and only found decreased mI : Cr in the frontal cortex of welders. In another study, reduced NAA : Cr was found only in the frontal cortex of Mn-exposed smelters, but not in the thalamus, putamen, or globus pallidus.[11] Additionally, a significant increase in GABA level, similar to the report of elevated GABA in globus pallidus tissue by Zwingmann *et al.*,[84] was observed in a larger thalamus-centered volume of interest in the same study.[11] This finding of increased thalamic GABA has been reproduced in additional populations of smelters and welders in different countries and

settings;[88–90] moreover, thalamic GABA levels were recently found to predict fine motor performance in Mn-exposed workers.[89] Finally, Long *et al.* also reported reduced Glu in the frontal cortex of Mn-exposed smelters and welders *vs*. matched controls, as well as reduced mI in the thalamus and posterior cingulate cortex.[16]

The wide range of metabolite changes reported in these studies most likely can be explained by differences in Mn-exposure settings and brain regions explored, as well as different scan and analysis protocols. However, a general trend is a decrease in NAA, especially at higher exposure settings such as in animal models or the smelter population reported by Dydak *et al.*,[11] in line with dysfunction or even degeneration of neurons. Another interesting aspect is the fact that many MRS studies report metabolic changes in the frontal cortex, supporting the notion that cortical areas, in particular the frontal cortex, are involved in and vulnerable to Mn neurotoxicity.

19.2.5 Diffusion Weighted Imaging

Diffusion weighted imaging (DWI) and diffusion tensor imaging (DTI) are forms of MRI based upon the Brownian motion of water molecules (diffusion).[91] Tissue cellularity and the presence of intact cell membranes limit the diffusion of water in tissue. The overall magnitude of diffusion is measured in terms of the mean diffusivity (MD) or apparent diffusion coefficient (ADC) while the fractional or relative anisotropy (FA or RA) represents the main vector or direction of water molecule diffusion within a voxel of tissue.[92] Changes in the MD, ADC and FA represent disruption in the movement of water secondary to changes in cellular architecture,[91] and all have been reported in association with Mn neurotoxicity. McKinney *et al.*[93] first reported restricted diffusion in the globus pallidus of a patient with Mn neurotoxicity secondary to liver failure and long-term TPN administration. Similarly, Criswell *et al.*[9] reported lower ADC values in the globus pallidus ($p = 0.04$) and anterior putamen ($p = 0.005$) of 18 Mn-exposed welders when compared to age- and sex-matched non-exposed controls. Both studies found the restricted diffusion in areas of gray matter with elevated *T*1-weighted intensity indices. Interestingly, in the study by Criswell *et al.* these changes were present in welders without symptomatic complaints and only minimal parkinsonian signs on examination.

Kim *et al.* reported a reduction in the FA of the corpus callosum and frontal white matter in Mn-exposed welders that correlated with elevated blood Mn levels, pallidal indices, and impaired neurobehavioral performance, suggesting that Mn also affects the microstructural abnormalities in white matter.[94] Specifically, digit span (backward), verbal fluency, Stroop's, and motor test outcomes were significantly associated with FA changes in the corpus callosum and frontal white matter. Finally, Stepens *et al.* reported both a diffuse decrease in white matter FA and an increase of 7% in average mean diffusivity within the bilateral globus pallidus in patients with

symptomatic Mn neurotoxicity secondary to intravenous methcathinone (ephedrone) abuse.[95] This differs from the restricted diffusion reported in the basal ganglia by McKinney *et al.*[93] and Criswell *et al.*[9] It is possible the different patterns of diffusion are secondary to differences in the underlying mechanisms of Mn neurotoxicity associated with occupational exposure, liver dysfunction, and ephedrone abuse. However, Favrole *et al.*[96] provide an interesting alternative hypothesis in their study of Wilson's disease. Wilson's disease is a genetic disorder of copper metabolism resulting in a similar clinical phenotype of parkinsonism and dystonia secondary to copper deposition within the basal ganglia. They found that subjects with pre-symptomatic Wilson's disease demonstrated restricted diffusion in the putamen, whereas symptomatic Wilson's disease was associated with increased putamen ADC values. Favrole *et al.*[96] hypothesized that this may represent an inflammatory processes or gliosis with increased cellularity preceding the typical degenerative lesions usually seen at autopsy.[96] Similarly, the difference in gray matter diffusivity may represent a spectrum of evolving inflammatory and destructive lesions in Mn neurotoxicity. Further studies in asymptomatic and symptomatic Mn neurotoxicity would be required to test this hypothesis.

19.2.6 Functional MRI

Functional MRI (fMRI) is an MRI technique that images brain activity by assessing changes in blood oxygenation and flow in response to neural activity – also called the hemodynamic response.[97–99] It is based on the fact that active brain areas will consume more oxygen, and that the regional blood flow is increased to meet this increased oxygen need. Given that oxygenated (Hb) and deoxygenated hemoglobin (dHb) have different magnetic properties, being paramagnetic and diamagnetic, respectively, the replacement of dHb by Hb will create a short ($\sim$5 s) increase in signal upon a stimulus, which can be detected by specialized MRI sequences and data processing. The fMRI images are usually presented in form of brain activation maps that show the brain areas that are active in response to a particular task or mental process. These maps are quantitative and thus can show whether certain brain regions are recruited less or more in a particular population.

Two studies have been conducted to date on Mn-exposed human subjects using fMRI to evaluate functional correlates of Mn-induced brain dysfunction. A first study investigated motor-related brain activation in Mn-exposed welders. Using a finger-tapping paradigm, the authors found increased activation of the primary sensorimotor cortex, bilateral supplementary motor area (SMA), bilateral premotor cortex, bilateral superior parietal cortex and ipsilateral dentate nucleus in the exposed group.[100] Furthermore, motor behavior, as measured by the Grooved Pegboard test of the right hand, correlated with the bilateral activation signal in the SMA obtained during finger tapping of the right hand.[100] The second study used

the 2-back verbal memory task to look at neural correlates of working memory alterations due to Mn exposure in the same cohort of welders.[101] While task performance showed no difference between exposed and non-exposed groups, the working memory networks of welders were significantly more activated and welders recruited additional brain regions for this task, such as the inferior frontal cortex, basal ganglia (including the putamen) and the cerebellum. Again, correlations between brain activity and cognitive testing outside the MRI scanner were found.[101] In summary these two studies not only confirm subclinical deficits in motor and cognitive function due to Mn exposure, but also suggest that Mn-exposed subjects activate common networks to a higher degree, and engage additional brain networks to perform the same task when compared with non-exposed subjects, possibly as a compensatory mechanism.

19.3 PET and SPECT Imaging

Positron emission tomography (PET) is a non-invasive functional imaging technique used to create three-dimensional images of the biochemical processes in the living brain. The PET system detects pairs of gamma rays indirectly emitted by a tracer labeled with a positron-emitting radionuclide; common examples include carbon-11 (^{11}C) and fluorine-18 (^{18}F). Multiple tracer molecules have been developed that target both general and specific biochemical sites including those within the pre- and postsynaptic dopaminergic nerve terminal. Fluorodeoxyglycose (^{18}F-FDG) is a general marker of tissue glucose uptake used in cancer screening and cerebral metabolisms studies.[102,103] Commonly used dopamine specific presynaptic radiotracers include tagged enzyme substrates such as 6-[^{18}F]fluoro-L-dopa and [β-^{11}C]-L-dopa (reflects aromatic L-amino acid decarboxylase activity[104]) and molecules with an affinity for dopamine presynaptic reuptake sites (also called dopamine transporter or DAT sites) including [^{11}C]-nomifensin, [^{11}C]-methylphenidate, and [^{11}C]-WIN.[105] Postsynaptic studies of the dopaminergic system commonly utilize tagged dopamine receptor ligands to measure dopamine receptor density. Studies in Mn neurotoxicity have primarily used the radiotracer [^{11}C]-raclopride which has an affinity for D2 post-synaptic dopamine receptors.[105] By combining radiotracer studies with specific biochemical targets, PET imaging can be used to pinpoint functional areas within pathways affected by neurodegenerative diseases and neurotoxic agents such as Mn to elucidate the underlying pathological mechanisms.

Just as with PET, single photon emission computed tomography (SPECT) may be used to assess dopamine neuron terminal markers. SPECT is similar to PET in its use of radioligands, which are chosen to bind to particular targets, and its detection of gamma rays emitted by the radioligand. In contrast to PET, SPECT tracers emit gamma radiation, which is measured directly with gamma cameras, resulting in lower spatial resolution ($\sim$1 cm resolution). However, SPECT scans utilize longer-lived and more easily obtained radioisotopes, making them less expensive than PET scans.

Dopamine transporter (DAT) SPECT has been utilized to study the integrity of the nigrostriatal dopaminergic system in both idiopathic Parkinson disease and manganese-induced parkinsonism.[106–109]

19.3.1 PET Studies in Non-Human Primates

Eriksson *et al.*[110] first used PET imaging in 1992 to study two monkeys exposed to manganese oxide by subcutaneous injections over a 16 month period. Both monkeys developed increased *T*1 intensities in the caudate, putamen, globus pallidus and internal capsule on MRI imaging and clinical signs of toxicity including unsteady gait, minor clumsiness of the hands, and hypoactivity. In both monkeys, uptake of striatal [^{11}C]-nomifensin (dopamine reuptake transporters) progressively declined to reach a 60% reduction from baseline. The first animal was also scanned with [β^{11}C]-L-dopa (pre-synaptic decarboxylase activity) and expressed normal uptake throughout the striatum. The second monkey underwent [^{11}C]-raclopride PET (D2 postsynaptic receptors) with the levels transiently decreased in the early stages of Mn intoxication, but normalized by the end of the study. The combination of the [β-^{11}C]-L-dopa and [^{11}C]-nomifensin data suggested that Mn toxicity caused either a loss of presynaptic dopamine nerves with a compensatory upregulation in decarboxylase activity and dopamine turnover or no change in the number of nerve terminals with a reduction in functional reuptake transporters. In either case, no definitive conclusions could be made from this small, initial study.

Next, Shinotoh *et al.*[111] performed the combination of [^{18}F]-fluoro-L-dopa and [^{11}C]-raclopride PET with [^{18}F]-fluoro-deoxyglucose PET (cerebral metabolic rate of glucose) before and after serial administration of 10–14 mg kg^{-1} of $MnCl_2$ to three adult male rhesus monkeys. After Mn administration one monkey demonstrated elevated *T*1 signal intensity in the caudate and putamen with hypoactivity and dystonic posturing. A second monkey demonstrated similar clinical findings but normal MRI imaging. The last monkey demonstrated no clinical or imaging findings of Mn neurotoxicity. However all monkeys were reported to have cell loss and gliosis in the globus pallidus and substantial nigra pars reticularis. There was no significant alteration in the cerebral metabolic rate of glucose as measured by [^{18}F]-fluoro-deoxyglucose PET. Similarly there was no change in [^{11}C]-raclopride or [^{18}F]-fluoro-deoxyglucose, suggesting preservation of the nigrostriatal dopaminergic pathway, despite clinical deficits and neuropathic changes in the globus pallidus.

More recently, Guilarte *et al.*[112,113] performed a series of studies in 13 adult male macaques administered serial intravenous (i.v.) injections of manganese sulfate at 3.3–5.0 mg Mn kg^{-1}, 5.0–6.7 mg Mn kg^{-1}, or 8.3–10.0 mg Mn kg^{-1} for 7–59 weeks and two imaging control monkeys. PET studies including [^{11}C]-methylphenidate (dopamine reuptake transporters), [^{11}C]-raclopride (D2 postsynaptic receptors) and [^{11}C]-raclopride with amphetamine challenge (*in vivo* dopamine release) were performed at baseline

and during chronic Mn exposure. Mn exposures did not affect dopamine transporters as measured by [^{11}C]-methylphenidate binding potential. The D2 postsynaptic dopamine receptors expressed a small but significant decrease (14.5%) in [^{11}C]-raclopride binding potential at 285 days post Mn administration. However, the primary finding of this study was a 51% decrease of amphetamine-induced dopamine release at 285 days post Mn administration relative to baseline.[112,113] The marked decrease in amphetamine-induced dopamine release was associated with a subtle decrease in fine motor skills and the general activity levels of the animals.[112,114] These studies also included post-mortem tissue analysis demonstrating no effect of Mn exposure on dopamine transport levels, D2 receptors, tyrosine hydroxylase levels, and dopamine or HVA (a dopamine metabolite) concentrations, indicating that the dopaminergic presynaptic terminals in the striatum were intact. Mn exposure in these animals appeared to cause changes in amphetamine-induced dopamine release without obvious nigrostriatal terminal degeneration.

Concurrently, Chen *et al.*[115] found that administration of high dose $MnSO_4$ caused an acute but transient increase in striatal dopamine transport levels measured by [^{11}C]-WIN 35,428 PET in two adult baboons. As part of this study they also demonstrated that acute Mn administration inhibits *in vitro* binding of [^{3}H]-WIN 35,428 to dopamine transporters in rat striatal membranes and uptake of [^{3}H]-DA by dopamine transporters into rat striatal synaptosomes, suggesting that the transient increase of [^{11}C]-WIN 35,428 (dopamine transporters) may be a compensatory response to its inhibitory effect on the transporter. This acute effect of Mn on dopamine transporter levels is different from the decreased DAT levels found after 16 months of repeat Mn exposure by Eriksson *et al.*[110] and the normal dopamine transporter levels described by Guilarte *et al.*[112] It seems likely the differences in these effects may be due to the duration of Mn exposure.

The PET studies from non-human primate models suggest that Mn neurotoxicity is mediated by presynaptic mechanisms that inhibit dopamine release, causing dysfunction but not degeneration of the nigrostriatal pathway. Differences between individual PET studies may be related to the variation in duration and magnitude of Mn exposure. However, the duration of exposure in all the non-human primate studies is limited (days *vs*. years) relative to typical occupational Mn exposures in humans. Therefore these PET findings may still represent early/transient changes in dopamine synapses, and the possibility of progressive nerve terminal degeneration or neuronal injury after chronic Mn exposure cannot be excluded. Further, these studies report striatal findings as a whole; individual differences between the caudate nucleus and putamen cannot be elucidated.

19.3.2 PET Studies in Human Subjects

The first PET study in Mn-exposed humans was completed by Wolters *et al.*[116] in four Taiwanese smelter workers with high levels of Mn exposure

and clinical parkinsonism. All four patients exhibited masked facies, bradykinesia, and gait abnormalities with two patients demonstrating rest tremor. Initial [18F]-fluorodopa PET (presynaptic decarboxylase activity) in these subjects demonstrated normal uptake in the caudate and putamen. Eight years later, the same subjects underwent repeat [^{18}F]-fluoro-L-dopa studies with [11C]-raclopride PET added to examine postsynaptic D2-dopamine receptors.[117] [18F]-fluoro-L-dopa uptake remained normal in all subjects despite progression of their parkinsonian symptoms. [11C]-raclopride binding was mildly reduced in the caudate and normal in the putamen, suggesting that the nigrostriatal pathway is not affected by Mn exposure.

In contrast, Kim *et al.*[118] performed [^{18}F]-fluoro-L-dopa PET on a parkinsonian welder with a 10 year history of welding exposure and elevated *T*1 MR signal in the globus pallidus. [^{18}F]-fluoro-L-dopa uptake was reduced in the left putamen. In addition, Racette *et al.*[119] describe two additional parkinsonian welders with Mn exposure. They found reduced [^{18}F]-fluoro-L-dopa uptake across the striatum with the greatest reduction in the posterior putamen, similar to the ranges and anatomical uptake patterns of the comparison group of early idiopathic Parkinson (IPD) subjects. Together these studies argue that Mn does affect function within the presynaptic dopaminergic neurons of exposed subjects.

Two studies have reported on [^{18}F]-fluoro-L-dopa PET in Mn neurotoxicity secondary to liver dysfunction and impaired biliary clearance. Racette *et al.*[120] reported reduced [^{18}F]-fluoro-L-dopa PET uptake in the caudate and putamen of a patient with severe parkinsonism in the setting of alcoholic cirrhosis, elevated blood Mn levels, and increased *T*1-weighted MR signal in the globus pallidum. [^{18}F]-fluoro-L-dopa uptake was reduced across the caudate, anterior, and posterior putamen within the range demonstrated by comparison subjects with IPD. However [^{18}F]-fluoro-L-dopa uptake in the caudate nucleus appeared to be relatively more affected in the cirrhotic patient with a caudate : posterior putamen uptake ratio of 1.43 compared to the mean IPD uptake ratio of 2.86. Criswell *et al.*[121] reported on another individual with Mn neurotoxicity secondary to alcoholic cirrhosis but mild parkinsonism in the setting of elevated blood Mn levels and MR pallidal signal. [^{18}F]-fluoro-L-dopa uptake was reduced across the striatum by more than two standard deviations (caudate, 24.7%; anterior putamen, 28.0%; posterior putamen, 29.3%) compared to healthy controls. [^{18}F]-fluoro-L-dopa again appeared to be more evenly affected across the striatum with a caudate : posterior putamen ratio of 0.99. Both studies indicate presynaptic dysfunction in Mn neurotoxicity secondary to liver dysfunction.

Sikk *et al.*[122] performed FDG PET in four former ephedrone addicts with extrapyramidal symptoms after long-term intravenous use of ephedrone (methcathinone) contaminated with high concentrations of Mn. All patients demonstrated a widespread, but heterogeneous, pattern of reduced FDG uptake within the basal ganglia and the surrounding white matter. However, it is unclear whether these changes are specific to Mn or related to long-term ephedrone abuse.

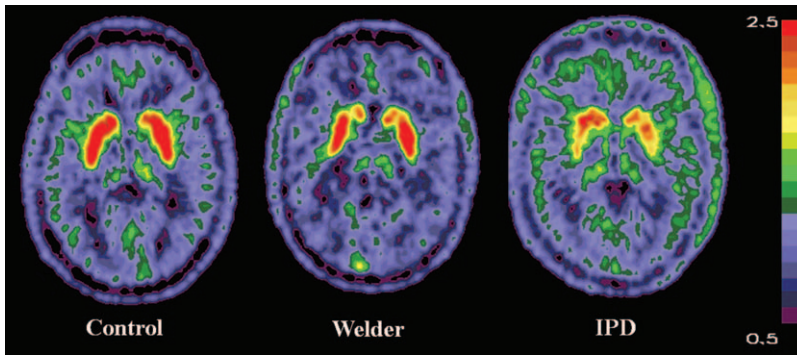

Figure 19.6 FDOPA PET composite images of decay-corrected counts from 24–94 minutes from a representative control, welder, and subject with idiopathic Parkinson disease (IPD) normalized to the reference region. FDOPA uptake is reduced in the caudate region of the welder in comparison to the control subject, while the posterior putamen is the most affected region in the subject with IPD.
(Reprinted from Neurology 76, S. Criswell, J. Perlmutter, T. Videen, S.Moerlein, H. Flores, A. Birke, B. Racette. Reduced uptake of [^{18}F]FDOPA PET in asymptomatic welders with occupational manganese exposure, pp. 1296–1301, Copyright 2011, with permission from Wolters Kluwer Health.)

One major confound common to all these initial human PET studies on symptomatic Mn neurotoxicity is the inability to differentiate subjects with IPD or, more recently, ephedrone use and superimposed Mn exposure from those with only Mn neurotoxicity. A recent study by Criswell *et al.*[123] eliminated this confound by performing [^{18}F]-fluoro-L-dopa PET in 20 asymptomatic welders exposed to Mn fumes. They found that caudate [^{18}F]-fluoro-L-dopa PET uptake was reduced by 11.71% in asymptomatic welders compared to control subjects ($p \leq 0.002$); this was slightly higher than the 17% reduction seen in the symptomatic IPD subjects (Figure 19.6). This finding has significance for two reasons. First, the presence of reduced [^{18}F]-fluoro-L-dopa caudate uptake in asymptomatic welders may represent a useful, early marker of Mn neurotoxicity in humans. Second, the preferential effect on caudate [^{18}F]-fluoro-L-dopa uptake was anatomically reversed from the pattern in IPD subjects (Figure 19.6). In combination with the previous studies by Racette *et al.*[120] and Criswell *et al.*,[121] this suggests that Mn in humans has a unique pattern of neurotoxicity. A previous case series collected by Bhatia and Marsden[124] report that lesions in the putamen are more likely to cause motor symptoms, while caudate lesions are more often associated with psychiatric and cognitive changes. This could explain the clinical phenotype associated with Mn neurotoxicity in which neuropsychiatric symptoms, including cognitive impairment, depression, and hallucinations, are often present before or concurrent with motor symptomatology, which would be unusual in early IPD.[125–127]

The differences between early PET studies by Wolters *et al.*[116] and subsequent studies may be related to differences in the method of Mn exposure, upgrades in scanner resolution, or more likely sample size, because these studies were not powered to detect the approximately 10% difference in [^{18}F]-fluoro-L-dopa uptake identified by Criswell *et al.*[123] While these [^{18}F]-fluoro-L-dopa PET studies demonstrate evidence of presynaptic dopaminergic dysfunction, [^{18}F]-fluoro-L-dopa measurements alone cannot distinguish a neurotoxic effect on nigrostriatal neurons from a dysfunctional process causing a regulatory effect on presynaptic decarboxylase activity. In combination with the non-human primate studies by Guilarte *et al.*,[112] these findings support the hypothesis that chronic Mn exposure produces clinical neurotoxicity through presynaptic dopamine terminal dysfunction. However, determining the specific presynaptic mechanism responsible for Mn neurotoxicity uptake in humans will require further research.

19.3.3 SPECT Studies

Various ligands binding to DAT, such as Tc-TRODAT-1, [123I]-β-CIT, [123I]-FP-CIT and [123I]-ioflupane, have been used to study presynaptic dopaminergic function in Mn-exposed workers,[106–108] Mn neurotoxicity in the context of severe liver dysfunction,[33] and patients exposed to Mn through their ephedrone addiction.[46,49,122] While SPECT has shown a progressive loss of DAT density in PD patients,[109] DAT studies in Mn exposure have been mixed. An early SPECT study demonstrated significantly reduced DAT levels in the striatum of two Mn-exposed workers by [123I]-β-CIT.[108] However, a subsequent report in four patients with chronic Mn intoxication from a ferromanganese smelting plant identified only mildly reduced DAT in the putamen.[106,107] SPECT scanning in one subject with Mn accumulation secondary to severe liver disease demonstrated normal overall DAT uptake in the striatum with scattered small hypodense regions within the putamen.[33] SPECT 123I-Ioflupane (DaTscan GE) scans of ephedrone addicts with clinical symptoms of manganism report normal DAT uptake.[46,49,122] Sikk *et al.* further performed iodine-123 iobenzamine (IBZM) SPECT to measure the density of dopamine D2 receptors in their cohort of ephedrone addicts.[45] They found normal tracer uptake in the striatum, indicating preserved postsynaptic D2 receptors, which suggests that manganism in ephedrone users may be related to dopaminergic dysfunction rather than degeneration, as suggested by Guilarte.[128]

There are several possible causes for the range of SPECT results in Mn neurotoxicity. First, the differences may be secondary to the underlying etiologies of Mn neurotoxicity (occupational exposure, liver failure, and contaminated ephedrone). Second, SPECT studies to date have been limited to symptomatic individuals, therefore confounding with early IPD, liver failure, or long-term ephedrone abuse cannot be eliminated. Lastly, detecting small or subtle differences may be difficult owing to the inherent limitations in the resolution of SPECT imaging. Future SPECT studies in larger cohorts

may help to further interpret SPECT imaging in these Mn-exposed cohorts and elucidate the underlying mechanisms of Mn neurotoxicity.

19.4 X-Ray Fluorescence

X-ray fluorescence (XRF) may be used for elemental imaging, which means it is a direct measure of tissue quantities of a particular chemical element, *e.g.* Mn. This type of direct measurement of tissue Mn makes it unique compared to all other imaging methods discussed in this chapter, which image Mn indirectly, as in MRI, or which image effects of Mn exposure on the body's biochemistry, as in PET and SPECT. To date XRF has found its applications in the study of Mn neurotoxicity in single cell imaging,[129–132] as well as in high-resolution (order of microns) elemental imaging of *ex vivo* brain slices of rats exposed to Mn.[133–135]

The generation of an XRF signal begins with the expulsion of a core electron (*e.g.* 1s) from the atomic shell by an incoming X-ray. The core hole produced in this process is rapidly filled by an electron from a higher orbital (*e.g.* 2p, 3p) while emitting a photon with an energy specific to the difference in orbital energy levels. Since every element has a unique orbital structure, peak locations of the resulting energy spectrum indicate the presence of a given element in the sample and peak height is proportional to the concentration of said element. To perform XRF imaging, a sample is raster scanned across a focused X-ray beam while an energy sensitive detector records the fluorescence spectrum on a pixel-by-pixel basis. Recorded data can then be fitted and elemental maps constructed. X-ray beams can be focused to several microns to provide imaging of large areas such as coronal sections of rodent or human brain. Alternately, focusing on a nanometer scale (currently down to 30 nm) allows for single cell imaging. While in principle Mn should be detectable at 30 nm resolution, practical considerations, such as image acquisition time, influence the choice of resolution. In addition to requiring a synchrotron source to perform measurements, XRF imaging of tissue is performed *ex vivo* and therefore cannot be used to study kinetics of metal uptake. Furthermore, sample drying and/or radiation damage prevents imaging of the same sample by a secondary method, such as immuno-histochemical staining.

Measuring Mn in single cells by XRF was reported as early as 2003,[129] followed by studies on Mn accumulation in dopaminergic cells of the Golgi apparatus.[131] The same authors, Carmona *et al.*,[136] recently used single cell micro-XRF to compare the cytotoxicity towards dopamine-producing cells of several environmental Mn sources: inorganic compounds of different oxidation state and solubility ($MnCl_2$, $MnSO_4$, and Mn_2O_3) and organic compounds (MMT, a gasoline additive, and maneb, a diththiocarbamate fungicide). The authors found that maneb exhibited the highest toxicity, followed by $MnCl_2$, $MnSO_4$ and MMT with intermediate toxicity, whereas the insoluble Mn_2O_3 was the least toxic compound.[136] The micro-XRF

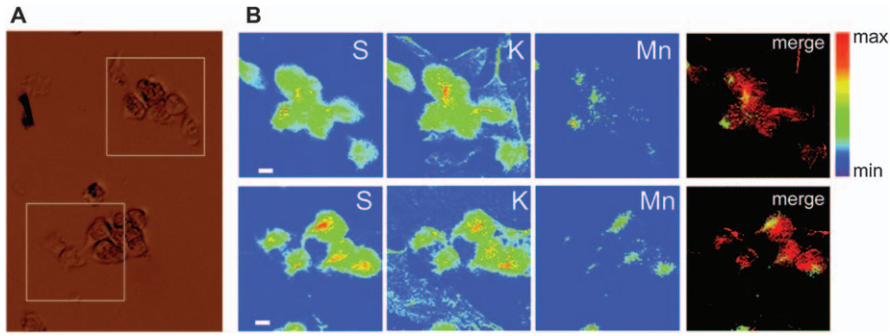

Figure 19.7 (A) Optical image of PC12 cells in culture exposed to 500 μM $MnCl_2$ during 24 h. White squares (100 μm×100 μm) indicate the two groups of cells analyzed by micro-XRF. (B) Maps of chemical element distributions (S, K and Mn) obtained by micro-SXRF and merged image of K (red) and Mn (green) distributions showing the perinuclear localization of Mn. Scale bar (white bar in sulfur images): 10 μm.
(Reproduced from Carmona, A. *et al.*, *Metallomics*, 2014, **6**, 822, with permission from the Royal Society of Chemistry.)

imaging technique used in this study enabled the creation of Mn, sulfur (S) and potassium (K) distribution maps within single cells with a resolution of 1 μm×1 μm, revealing a perinuclear localization of Mn in cells exposed to $MnCl_2$ (Figure 19.7).

Recently XRF has also been used to image whole brain slices from rodents exposed to Mn (Figure 19.8).[133–135] The penetrating nature of X-rays allows for relatively thick sections (*e.g.* 30 μm), and the technique is sensitive to the total metal content regardless of the binding environment. Robison *et al.* used XRF imaging to investigate the spatial and quantitative distribution of Mn relative to other biologically relevant metal ions, such as Fe, copper or zinc, in brains of rats chronically exposed to Mn. They found that Mn did not follow the distribution of any of these metals in the brain, with highest Mn concentrations in the globus pallidus, substantia nigra compacta and the thalamus.[135] Subsequently they investigated spatial correlations between Mn and Zn, as well as Mn and Fe, in exposed brain slices of the hippocampal formation both at the tissue level (40 μm×40 μm) and the cellular level (300 nm×300 nm).[134]

Most noteworthy is the comparison of some of the high-resolution imaging techniques described in this chapter. Daoust *et al.*[133] studied the Mn distribution within the rat hippocampus by XRF, comparing an intracranial to an intraperitoneal route of Mn, and correlated the XRF results to the MEMRI signal. His results are important in validating MEMRI as quantitative measure by finding a clear correlation between the Mn-enhanced MRI contrast in MEMRI and the total amount of Mn measured by XRF, demonstrating in addition that MEMRI is sensitive to low Mn concentrations (Figure 19.9).

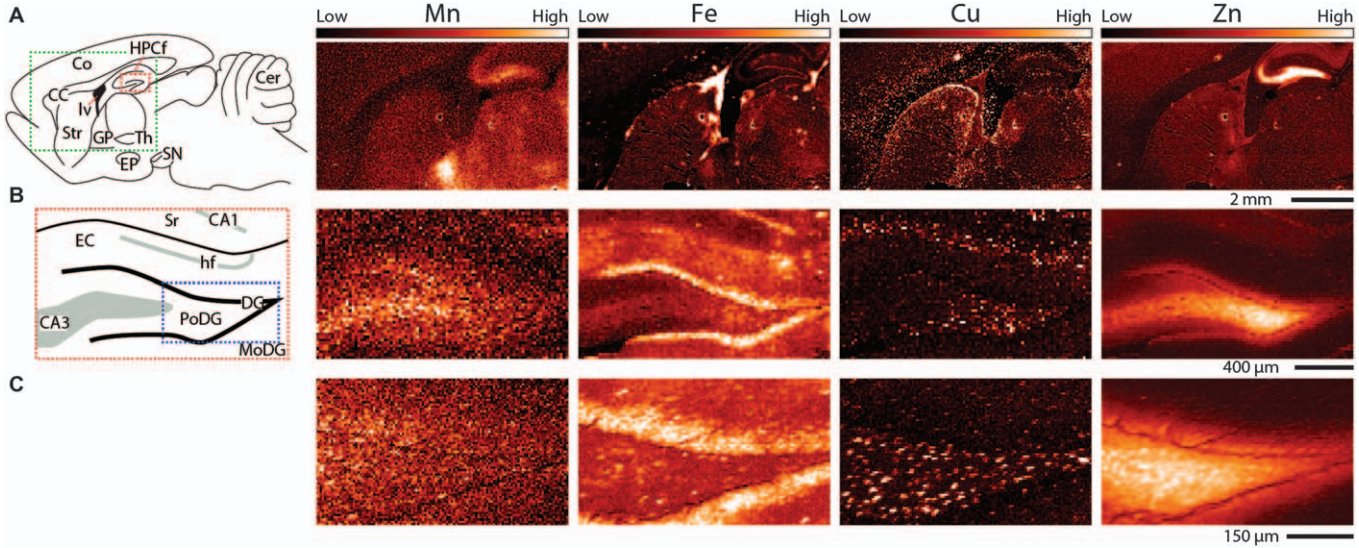

Figure 19.8 XRF images of Mn, Fe, Cu and Zn in a 30 μm thick sagittal section of the brain of a rodent chronically exposed to Mn, showing different resolutions. (A) Diagram of the sagittal section (lateral ~1.90 mm) imaged by XRF at "tissue level" resolution (40 μm×40 μm pixel size) displayed to the right. The scale bar on the right represents a length of 2 mm, and the green dashed box in the diagram represents the approximate location of tissue level XRF imaging. CC, corpus callosum; Cer, cerebellum; Co, cortex; EP, entopeduncular nucleus; HPCf, hippocampal formation; lv, lateral ventricle; SN, substantia nigra; Str, striatum; Th, thalamus. (B) Higher resolution image (20 μm×20 μm pixel size) taken of the HPCf which demonstrates heterogeneous distribution of transition metals. The red dashed box in schematic (A) indicates the approximate location of the scan. Scale bar represents a length of 400 μm. CA1 & 3, cornus ammonis 1 & 3; DG, granular layer of the dentate gyrus; EC, entorhinal cortex; hf, hippocampal fissure; MoDG/PoDG, molecular/polymorphic layer of the dentate gyrus; Sr, striatum radiatum. (C) Highest resolution image (5 μm×5 μm pixel size) of the crest of the DG, indicated by the blue dashed box in the schematic displayed in (B). The scale bar represents a length of 150 μm.
(Data courtesy of Pushkar Y, Sullivan B, and Robison G, Purdue University.)

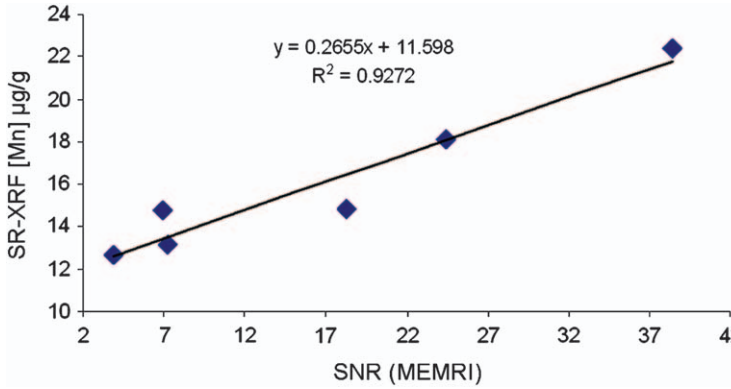

Figure 19.9 Signal to noise ratio (SNR) in MEMRI imaging as a function of Mn concentration determined by XRF. Each point represents one animal. The line represents a linear fit to the data.
(Reprinted from NeuroImage 64, A. Daoust, E. L. Barbier, S. Bohic, Manganese enhanced MRI in rat hippocampus: A correlative study with synchrotron X-ray microprobe, Pages 10–18, Copyright 2013, with permission from Elsevier.)

19.5 Conclusions

In summary, a wide range of imaging modalities has been used successfully to measure and study the effects of Mn exposure *in vivo*. Notably, all of these imaging studies have focused on the brain and thus on the neurotoxic aspects of Mn. MRI (*T*1-weighted imaging, relaxometry and MEMRI) as well as XRF may be used to study the accumulation and deposition of Mn in tissue, ranging from millimeter resolution in humans using MRI to subcellular micrometer resolution in *ex vivo* tissue extracts using XRF. On the other hand, ''functional'' imaging techniques such as PET, SPECT, MRS, DWI, fMRI and MR volumetry have been shown to be useful tools for studying the toxic effects of Mn exposure on neurochemistry, neurotransmitter systems, neuronal and axonal integrity, and ultimately neurodegeneration. These methods allow investigation of the mechanism of neurotoxicity, and monitoring of disease progression or response to potential treatment.

In all of these imaging studies, the limitations of the applied methods, *e.g.* in spatial resolution or sensitivity, as well as the specificity of the techniques, need to be taken into account when interpreting the data. Note that none of the techniques discussed in this chapter that can be applied *in vivo* gives a direct measurement of the quantity of interest. For example, *T*1-weighted MRI does not measure Mn itself, but rather hydrogen nuclei, whose relaxation properties are changed by close proximity to paramagnetic Mn ions. To complicate matters, proximity to other paramagnetic metals such as Fe may also contribute to the same contrast mechanism. Another example is PET imaging, which does not directly measure neurodegeneration itself, but rather binding at presynaptic dopamine transporter sites or postsynaptic

dopamine receptors. Finally, the choice of imaging parameters may greatly influence the variability in results from different studies, as they influence sensitivity and specificity.

Over the past few years, several very good and detailed review articles have been written about neuroimaging of Mn toxicity by Kim *et al.*[137] and Fitsanakis *et al.*[138] (who focused on MRI), as well as portions of more general reviews by Aschner[139] and Guilarte.[128] Technological developments in neuroimaging are advancing rapidly, and more sophisticated imaging methodology is becoming more widely available to study the effects of Mn neurotoxicity. This trend is likely to increase in coming years, yielding higher resolution both *in vivo* and *in vitro* or the ability to assess a wider range of functional and biochemical measures of toxicity.

Acknowledgements

The authors want to thank James B. Murdoch for careful proof reading and discussions, and Zaiyang Long, Ruoyun Ma and Chien-Lin Yeh for assistance in putting together this chapter. We further acknowledge funding from NIH R01 ES020529 (Dydak) and NIH K23ES021444-01 (Criswell).

References

1. M. H. Mendonca-Dias, E. Gaggelli and P. C. Lauterbur, Paramagnetic contrast agents in nuclear magnetic resonance medical imaging, *Semin. Nucl. Med.*, 1983, **13**, 364–376.
2. Y. S. Kang and J. C. Gore, Studies of tissue NMR relaxation enhancement by manganese. Dose and time dependences, *Invest. Radiol.*, 1984, **19**, 399–407.
3. C. F. Geraldes, A. D. Sherry, R. D. Brown, 3rd and S. H. Koenig, Magnetic field dependence of solvent proton relaxation rates induced by Gd^{3+} and Mn^{2+} complexes of various polyaza macrocyclic ligands: implications for NMR imaging, *Magn. Reson. Med.*, 1986, **3**, 242–250.
4. D. A. Cory, D. J. Schwartzentruber and B. H. Mock, Ingested manganese chloride as a contrast agent for magnetic resonance imaging, *Magn. Reson. Imaging*, 1987, **5**, 65–70.
5. D. Fornasiero, J. C. Bellen, R. J. Baker and B. E. Chatterton, Paramagnetic complexes of manganese(II), iron(III), and gadolinium(III) as contrast agents for magnetic resonance imaging. The influence of stability constants on the biodistribution of radioactive aminopolycarboxylate complexes, *Invest. Radiol.*, 1987, **22**, 322–327.
6. A. C. Silva, J. H. Lee, I. Aoki and A. P. Koretsky, Manganese-enhanced magnetic resonance imaging (MEMRI): methodological and practical considerations, *NMR Biomed.*, 2004, **17**, 532–543.
7. W. J. Zhang, Z. L. Liu and H. Shao, [Biomarkers of workers exposed to manganese], *Zhonghua Laodong Weisheng Zhiyebing Zazhi*, 2010, **28**, 926–928.

8. M. C. Newland, T. L. Ceckler, J. H. Kordower and B. Weiss, Visualizing manganese in the primate basal ganglia with magnetic resonance imaging, *Exp. Neurol.*, 1989, **106**, 251–258.
9. S. R. Criswell, J. S. Perlmutter, J. L. Huang, N. Golchin, H. P. Flores, A. Hobson, M. Aschner, K. M. Erikson, H. Checkoway and B. A. Racette, Basal ganglia intensity indices and diffusion weighted imaging in manganese-exposed welders, *Occup. Environ. Med.*, 2012, **69**, 437–443.
10. M. C. Dietz, W. Wrazidlo, A. Ihrig, M. Bader and G. Triebig, [Magnetic resonance tomography of the brain in workers with chronic occupational manganese dioxide exposure], *Rofo*, 2000, **172**, 514–520.
11. U. Dydak, Y. M. Jiang, L. L. Long, H. Zhu, J. Chen, W. M. Li, R. A. Edden, S. Hu, X. Fu, Z. Long, X. A. Mo, D. Meier, J. Harezlak, M. Aschner, J. B. Murdoch and W. Zheng, In vivo measurement of brain GABA concentrations by magnetic resonance spectroscopy in smelters occupationally exposed to manganese, *Environ. Health Perspect.*, 2011, **119**, 219–224.
12. Y. Jiang, W. Zheng, L. Long, W. Zhao, X. Li, X. Mo, J. Lu, X. Fu, W. Li, S. Liu, Q. Long, J. Huang and E. Pira, Brain magnetic resonance imaging and manganese concentrations in red blood cells of smelting workers: search for biomarkers of manganese exposure, *Neurotoxicology*, 2007, **28**, 126–135.
13. K. A. Josephs, J. E. Ahlskog, K. J. Klos, N. Kumar, R. D. Fealey, M. R. Trenerry and C. T. Cowl, Neurologic manifestations in welders with pallidal MRI T1 hyperintensity, *Neurology*, 2005, **64**, 2033–2039.
14. Y. Kim, High signal intensities on T1-weighted MRI as a biomarker of exposure to manganese, *Ind. Health*, 2004, **42**, 111–115.
15. Y. Kim, K. S. Kim, J. S. Yang, I. J. Park, E. Kim, Y. Jin, K. R. Kwon, K. H. Chang, J. W. Kim, S. H. Park, H. S. Lim, H. K. Cheong, Y. C. Shin, J. Park and Y. Moon, Increase in signal intensities on T1-weighted magnetic resonance images in asymptomatic manganese-exposed workers, *Neurotoxicology*, 1999, **20**, 901–907.
16. Z. Long, Y. M. Jiang, X. R. Li, W. Fadel, J. Xu, C. L. Yeh, L. L. Long, H. L. Luo, J. Harezlak, J. B. Murdoch, W. Zheng and U. Dydak, Vulnerability of welders to manganese exposure – A neuroimaging study, *Neurotoxicology*, 2014.
17. R. Lucchini, E. Albini, D. Placidi, R. Gasparotti, M. G. Pigozzi, G. Montani and L. Alessio, Brain magnetic resonance imaging and manganese exposure, *Neurotoxicology*, 2000, **21**, 769–775.
18. K. Nelson, J. Golnick, T. Korn and C. Angle, Manganese encephalopathy: utility of early magnetic resonance imaging, *Br. J. Ind. Med.*, 1993, **50**, 510–513.
19. A. H. Sadek, R. Rauch and P. E. Schulz, Parkinsonism due to manganism in a welder, *Int. J. Toxicol.*, 2003, **22**, 393–401.
20. K. Sato, H. Ueyama, R. Arakawa, T. Kumamoto and T. Tsuda, [A case of welder presenting with parkinsonism after chronic manganese exposure], *Rinsho shinkeigaku/Clin. Neurol.*, 2000, **40**, 1110–1115.

21. S. Sen, M. R. Flynn, G. Du, A. I. Troster, H. An and X. Huang, Manganese accumulation in the olfactory bulbs and other brain regions of ''asymptomatic'' welders, *Toxicol. Sci.*, 2011, **121**, 160–167.
22. R. F. Butterworth, L. Spahr, S. Fontaine and G. P. Layrargues, Manganese toxicity, dopaminergic dysfunction and hepatic encephalopathy, *Metab. Brain Dis.*, 1995, **10**, 259–267.
23. Y. Choi, J. K. Park, N. H. Park, J. W. Shin, C. I. Yoo, C. R. Lee, H. Lee, H. K. Kim, S. R. Kim, T. H. Jung, J. Park, C. S. Yoon and Y. Kim, Whole blood and red blood cell manganese reflected signal intensities of T1-weighted magnetic resonance images better than plasma manganese in liver cirrhotics, *J. Occup. Health*, 2005, **47**, 68–73.
24. R. A. Hauser, T. A. Zesiewicz, C. Martinez, A. S. Rosemurgy and C. W. Olanow, Blood manganese correlates with brain magnetic resonance imaging changes in patients with liver disease, *Can. J. Neurol. Sci.*, 1996, **23**, 95–98.
25. R. A. Hauser, T. A. Zesiewicz, A. S. Rosemurgy, C. Martinez and C. W. Olanow, Manganese intoxication and chronic liver failure, *Ann. Neurol.*, 1994, **36**, 871–875.
26. K. J. Klos, J. E. Ahlskog, K. A. Josephs, R. D. Fealey, C. T. Cowl and N. Kumar, Neurologic spectrum of chronic liver failure and basal ganglia T1 hyperintensity on magnetic resonance imaging: probable manganese neurotoxicity, *Arch. Neurol.*, 2005, **62**, 1385–1390.
27. D. Krieger, S. Krieger, O. Jansen, P. Gass, L. Theilmann and H. Lichtnecker, Manganese and chronic hepatic encephalopathy, *Lancet*, 1995, **346**, 270–274.
28. E. A. Malecki, A. G. Devenyi, T. F. Barron, T. J. Mosher, P. Eslinger, C. V. Flaherty-Craig and L. Rossaro, Iron and manganese homeostasis in chronic liver disease: relationship to pallidal T1-weighted magnetic resonance signal hyperintensity, *Neurotoxicology*, 1999, **20**, 647–652.
29. N. H. Park, J. K. Park, Y. Choi, C. I. Yoo, C. R. Lee, H. Lee, H. K. Kim, S. R. Kim, T. H. Jeong, J. Park, C. S. Yoon and Y. Kim, Whole blood manganese correlates with high signal intensities on T1-weighted MRI in patients with liver cirrhosis, *Neurotoxicology*, 2003, **24**, 909–915.
30. L. Spahr, R. F. Butterworth, S. Fontaine, L. Bui, G. Therrien, P. C. Milette, L. H. Lebrun, J. Zayed, A. Leblanc and G. Pomier-Layrargues, Increased blood manganese in cirrhotic patients: relationship to pallidal magnetic resonance signal hyperintensity and neurological symptoms, *Hepatology*, 1996, **24**, 1116–1120.
31. A. Rovira, J. Alonso and J. Cordoba, MR imaging findings in hepatic encephalopathy, *AJNR Am. J. Neuroradiol.*, 2008, **29**, 1612–1621.
32. J. Alonso, J. Cordoba and A. Rovira, Brain magnetic resonance in hepatic encephalopathy, *Seminars in ultrasound, CT, and MRI*, 2014, **35**, 136–152.
33. J. Kim, J. M. Kim, Y. K. Kim, J. W. Shin, S. H. Choi, S. E. Kim and Y. Kim, Dopamine transporter SPECT of a liver cirrhotic with atypical parkinsonism, *Ind. Health*, 2007, **45**, 497–500.

34. K. J. Klos, J. E. Ahlskog, N. Kumar, S. Cambern, J. Butz, M. Burritt, R. D. Fealey, C. T. Cowl, J. E. Parisi and K. A. Josephs, Brain metal concentrations in chronic liver failure patients with pallidal T1 MRI hyperintensity, *Neurology*, 2006, **67**, 1984–1989.
35. S. A. Mirowitz, T. J. Westrich and J. D. Hirsch, Hyperintense basal ganglia on T1-weighted MR images in patients receiving parenteral nutrition, *Radiology*, 1991, **181**, 117–120.
36. J. Ono, K. Harada, R. Kodaka, K. Sakurai, H. Tajiri, Y. Takagi, T. Nagai, T. Harada, A. Nihei, A. Okada, *et al.*, Manganese deposition in the brain during long-term total parenteral nutrition, *JPEN, J. Parenter. Enteral Nutr.*, 1995, **19**, 310–312.
37. Y. Kafritsa, J. Fell, S. Long, M. Bynevelt, W. Taylor and P. Milla, Long-term outcome of brain manganese deposition in patients on home parenteral nutrition, *Arch. Dis. Child.*, 1998, **79**, 263–265.
38. Y. Iinuma, M. Kubota, M. Uchiyama, M. Yagi, S. Kanada, S. Yamazaki, H. Murata, K. Okamoto, M. Suzuki and K. Nitta, Whole-blood manganese levels and brain manganese accumulation in children receiving long-term home parenteral nutrition, *Pediatr. Surg. Int.*, 2003, **19**, 268–272.
39. H. Suzuki, J. Takanashi, N. Saeki and Y. Kohno, Temporal parenteral nutrition in children causing t1 shortening in the anterior pituitary gland and globus pallidus, *Neuropediatrics*, 2003, **34**, 200–204.
40. R. Abdalian, O. Saqui, G. Fernandes and J. P. Allard, Effects of manganese from a commercial multi-trace element supplement in a population sample of Canadian patients on long-term parenteral nutrition, *JPEN, J. Parenter. Enteral Nutr.*, 2013, **37**, 538–543.
41. S. A. Mirowitz and T. J. Westrich, Basal ganglial signal intensity alterations: reversal after discontinuation of parenteral manganese administration, *Radiology*, 1992, **185**, 535–536.
42. R. M. de Bie, R. M. Gladstone, A. P. Strafella, J. H. Ko and A. E. Lang, Manganese-induced Parkinsonism associated with methcathinone (Ephedrone) abuse, *Arch. Neurol.*, 2007, **64**, 886–889.
43. Y. Sanotsky, R. Lesyk, L. Fedoryshyn, I. Komnatska, Y. Matviyenko and S. Fahn, Manganic encephalopathy due to ''ephedrone'' abuse, *Mov. Disord.*, 2007, **22**, 1337–1343.
44. K. Sikk, P. Taba, S. Haldre, J. Bergquist, D. Nyholm, G. Zjablov, T. Asser and S. M. Aquilonius, Irreversible motor impairment in young addicts–ephedrone, manganism or both?, *Acta Neurol. Scand.*, 2007, **115**, 385–389.
45. K. Sikk, S. Haldre, S. M. Aquilonius, A. Asser, M. Paris, A. Roose, J. Petterson, S. L. Eriksson, J. Bergquist and P. Taba, Manganese-induced parkinsonism in methcathinone abusers: bio-markers of exposure and follow-up, *Eur. J. Neurol.*, 2013, **20**, 915–920.
46. C. Colosimo and M. Guidi, Parkinsonism due to ephedrone neurotoxicity: a case report, *Eur. J. Neurol.*, 2009, **16**, e114–115.
47. A. Stepens, I. Logina, V. Liguts, P. Aldins, I. Eksteina, A. Platkajis, I. Martinsone, E. Terauds, B. Rozentale and M. Donaghy,

A Parkinsonian syndrome in methcathinone users and the role of manganese, *N. Engl. J. Med.*, 2008, **358**, 1009–1017.

48. F. Varlibas, I. Delipoyraz, G. Yuksel, G. Filiz, H. Tireli and N. O. Gecim, Neurotoxicity following chronic intravenous use of ''Russian cocktail'', *Clin. Toxicol.*, 2009, **47**, 157–160.
49. M. Selikhova, L. Fedoryshyn, Y. Matviyenko, I. Komnatska, M. Kyrylchuk, L. Krolicki, A. Friedman, A. Taylor, H. R. Jager, A. Lees and Y. Sanotsky, Parkinsonism and dystonia caused by the illicit use of ephedrone–a longitudinal study, *Mov. Disord.*, 2008, **23**, 2224–2231.
50. U. Dydak, J. Xu, A. Epur, X. Li, S. Streitmatter, L. L. Long, W. Zheng and Y. M. Jiang, Brain Regions showing Manganese Accumulation in the Human versus the Rat Brain, *Proc. Intl. Soc. Mag. Reson. Med.*, 2011, **19**, 1428.
51. T. R. Guilarte, J. L. McGlothan, M. Degaonkar, M. K. Chen, P. B. Barker, T. Syversen and J. S. Schneider, Evidence for cortical dysfunction and widespread manganese accumulation in the nonhuman primate brain following chronic manganese exposure: a 1H-MRS and MRI study, *Toxicol. Sci.*, 2006, **94**, 351–358.
52. D. C. Dorman, M. F. Struve, B. A. Wong, J. A. Dye and I. D. Robertson, Correlation of brain magnetic resonance imaging changes with pallidal manganese concentrations in rhesus monkeys following subchronic manganese inhalation, *Toxicol. Sci.*, 2006, **92**, 219–227.
53. R. E. London, G. Toney, S. A. Gabel and A. Funk, Magnetic resonance imaging studies of the brains of anesthetized rats treated with manganese chloride, *Brain Res. Bull.*, 1989, **23**, 229–235.
54. Y. T. Kuo, A. H. Herlihy, P. W. So, K. K. Bhakoo and J. D. Bell, In vivo measurements of T1 relaxation times in mouse brain associated with different modes of systemic administration of manganese chloride, *J. Magn. Reson. Imaging*, 2005, **21**, 334–339.
55. G. Discalzi, E. Pira, E. Herrero Hernandez, C. Valentini, M. Turbiglio and F. Meliga, Occupational Mn parkinsonism: magnetic resonance imaging and clinical patterns following CaNa2-EDTA chelation, *Neurotoxicology*, 2000, **21**, 863–866.
56. A. Takeda, J. Sawashita and S. Okada, Biological half-lives of zinc and manganese in rat brain, *Brain Res.*, 1995, **695**, 53–58.
57. D. C. Dorman, M. F. Struve, M. W. Marshall, C. U. Parkinson, R. A. James and B. A. Wong, Tissue manganese concentrations in young male rhesus monkeys following subchronic manganese sulfate inhalation, *Toxicol. Sci.*, 2006, **92**, 201–210.
58. M. C. Newland, C. Cox, R. Hamada, G. Oberdorster and B. Weiss, The clearance of manganese chloride in the primate, *Fundam. Appl. Toxicol.*, 1987, **9**, 314–328.
59. B. Gallez, R. Demeure, C. Baudelet, N. Abdelouahab, N. Beghein, B. Jordan, M. Geurts and H. A. Roels, Non invasive quantification of manganese deposits in the rat brain by local measurement of NMR proton T1 relaxation times, *Neurotoxicology*, 2001, **22**, 387–392.

60. E. Kim, Y. Kim, H. K. Cheong, S. Cho, Y. C. Shin, J. Sakong, K. S. Kim, J. S. Yang, Y. W. Jin and S. K. Kang, Pallidal index on MRI as a target organ dose of manganese: structural equation model analysis, *Neurotoxicology*, 2005, **26**, 351–359.
61. Y. Chang, S. T. Woo, Y. Kim, J. J. Lee, H. J. Song, H. J. Lee, S. H. Kim, H. Lee, Y. J. Kwon, J. H. Ahn, S. J. Park, I. S. Chung and K. S. Jeong, Pallidal index measured with three-dimensional T1-weighted gradient echo sequence is a good predictor of manganese exposure in welders, *J. Magn. Reson. Imaging*, 2010, **31**, 1020–1026.
62. S. H. Kim, K. H. Chang, J. G. Chi, H. K. Cheong, J. Y. Kim, Y. M. Kim and M. H. Han, Sequential change of MR signal intensity of the brain after manganese administration in rabbits. Correlation with manganese concentration and histopathologic findings, *Invest. Radiol.*, 1999, **34**, 383–393.
63. D. S. Choi, E. A. Kim, H. K. Cheong, H. S. Khang, J. W. Ryoo, J. M. Cho, J. Sakong and I. Park, Evaluation of MR signal index for the assessment of occupational manganese exposure of welders by measurement of local proton T1 relaxation time, *Neurotoxicology*, 2007, **28**, 284–289.
64. M. Ulla, J. M. Bonny, L. Ouchchane, I. Rieu, B. Claise and F. Durif, Is R2* a new MRI biomarker for the progression of Parkinson's disease? A longitudinal follow-up, *PLoS One*, 2013, **8**, e57904.
65. T. Inoue, T. Majid and R. G. Pautler, Manganese enhanced MRI (MEMRI): neurophysiological applications, *Rev. Neurosci.*, 2011, **22**, 675–694.
66. A. C. Silva and N. A. Bock, Manganese-enhanced MRI: an exceptional tool in translational neuroimaging, *Schizophr. Bull.*, 2008, **34**, 595–604.
67. A. P. Koretsky and A. C. Silva, Manganese-enhanced magnetic resonance imaging (MEMRI), *NMR Biomed.*, 2004, **17**, 527–531.
68. R. G. Pautler, A. C. Silva and A. P. Koretsky, In vivo neuronal tract tracing using manganese-enhanced magnetic resonance imaging, *Magn. Reson. Med.*, 1998, **40**, 740–748.
69. I. Aoki, C. Tanaka, T. Takegami, T. Ebisu, M. Umeda, M. Fukunaga, K. Fukuda, A. C. Silva, A. P. Koretsky and S. Naruse, Dynamic activity-induced manganese-dependent contrast magnetic resonance imaging (DAIM MRI), *Magn. Reson. Med.*, 2002, **48**, 927–933.
70. Y. J. Lin and A. P. Koretsky, Manganese ion enhances T1-weighted MRI during brain activation: an approach to direct imaging of brain function, *Magn. Reson. Med.*, 1997, **38**, 378–388.
71. T. Watanabe, O. Natt, S. Boretius, J. Frahm and T. Michaelis, In vivo 3D MRI staining of mouse brain after subcutaneous application of $MnCl_2$, *Magn. Reson. Med.*, 2002, **48**, 852–859.
72. I. Aoki, Y. J. Wu, A. C. Silva, R. M. Lynch and A. P. Koretsky, In vivo detection of neuroarchitecture in the rodent brain using manganese-enhanced MRI, *Neuroimage*, 2004, **22**, 1046–1059.
73. K. H. Chuang, A. P. Koretsky and C. H. Sotak, Temporal changes in the T1 and T2 relaxation rates (DeltaR1 and DeltaR2) in the rat brain are

consistent with the tissue-clearance rates of elemental manganese, *Magn. Reson. Med.*, 2009, **61**, 1528–1532.

74. K. H. Chuang and A. Koretsky, Improved neuronal tract tracing using manganese enhanced magnetic resonance imaging with fast T(1) mapping, *Magn. Reson. Med.*, 2006, **55**, 604–611.
75. N. A. Bock, F. F. Paiva and A. C. Silva, Fractionated manganese-enhanced MRI, *NMR Biomed.*, 2008, **21**, 473–478.
76. V. Bouilleret, L. Cardamone, C. Liu, A. S. Koe, K. Fang, J. P. Williams, D. E. Myers, T. J. O'Brien and N. C. Jones, Confounding neurodegenerative effects of manganese for in vivo MR imaging in rat models of brain insults, *J. Magn. Reson. Imaging*, 2011, **34**, 774–784.
77. Y. Chang, S. U. Jin, Y. Kim, K. M. Shin, H. J. Lee, S. H. Kim, J. H. Ahn, S. J. Park, K. S. Jeong, Y. C. Weon and H. Lee, Decreased brain volumes in manganese-exposed welders, *Neurotoxicology*, 2013, **37**, 182–189.
78. R. A. Edden and P. B. Barker, Spatial effects in the detection of gamma-aminobutyric acid: improved sensitivity at high fields using inner volume saturation, *Magn. Reson. Med.*, 2007, **58**, 1276–1282.
79. M. Mescher, H. Merkle, J. Kirsch, M. Garwood and R. Gruetter, Simultaneous in vivo spectral editing and water suppression, *NMR Biomed.*, 1998, **11**, 266–272.
80. P. G. Mullins, D. J. McGonigle, R. L. O'Gorman, N. A. Puts, R. Vidyasagar, C. J. Evans, Cardiff Symposium on MRS of GABA and R. A. Edden, Current practice in the use of MEGA-PRESS spectroscopy for the detection of GABA, *NeuroImage*, 2014, **86**, 43–52.
81. J. Pfeuffer, I. Tkac, S. W. Provencher and R. Gruetter, Toward an in vivo neurochemical profile: quantification of 18 metabolites in short-echo-time (1)H NMR spectra of the rat brain, *J. Magn. Reson.*, 1999, **141**, 104–120.
82. G. Oz, J. R. Alger, P. B. Barker, R. Bartha, A. Bizzi, C. Boesch, P. J. Bolan, K. M. Brindle, C. Cudalbu, A. Dincer, U. Dydak, U. E. Emir, J. Frahm, R. G. Gonzalez, S. Gruber, R. Gruetter, R. K. Gupta, A. Heerschap, A. Henning, H. P. Hetherington, F. A. Howe, P. S. Huppi, R. E. Hurd, K. Kantarci, D. W. Klomp, R. Kreis, M. J. Kruiskamp, M. O. Leach, A. P. Lin, P. R. Luijten, M. Marjanska, A. A. Maudsley, D. J. Meyerhoff, C. E. Mountford, S. J. Nelson, M. N. Pamir, J. W. Pan, A. C. Peet, H. Poptani, S. Posse, P. J. Pouwels, E. M. Ratai, B. D. Ross, T. W. Scheenen, C. Schuster, I. C. Smith, B. J. Soher, I. Tkac, D. B. Vigneron, R. A. Kauppinen and M. R. S. C. Group, Clinical proton MR spectroscopy in central nervous system disorders, *Radiology*, 2014, **270**, 658–679.
83. C. Zwingmann, D. Leibfritz and A. S. Hazell, Energy metabolism in astrocytes and neurons treated with manganese: relation among cell-specific energy failure, glucose metabolism, and intercellular trafficking using multinuclear NMR-spectroscopic analysis, *J. Cereb. Blood Flow Metab.*, 2003, **23**, 756–771.

84. C. Zwingmann, D. Leibfritz and A. S. Hazell, Nmr spectroscopic analysis of regional brain energy metabolism in manganese neurotoxicity, *Glia*, 2007, **55**, 1610–1617.
85. N. Just, C. Cudalbu, H. Lei and R. Gruetter, Effect of manganese chloride on the neurochemical profile of the rat hypothalamus, *J. Cereb. Blood Flow Metab.*, 2011, **31**, 2324–2333.
86. E. A. Kim, H. K. Cheong, D. S. Choi, J. Sakong, J. W. Ryoo, I. Park and D. M. Kang, Effect of occupational manganese exposure on the central nervous system of welders: 1H magnetic resonance spectroscopy and MRI findings, *Neurotoxicology*, 2007, **28**, 276–283.
87. Y. Chang, S. T. Woo, J. J. Lee, H. J. Song, H. J. Lee, D. S. Yoo, S. H. Kim, H. Lee, Y. J. Kwon, H. J. Ahn, J. H. Ahn, S. J. Park, Y. C. Weon, I. S. Chung, K. S. Jeong and Y. Kim, Neurochemical changes in welders revealed by proton magnetic resonance spectroscopy, *Neurotoxicology*, 2009, **30**, 950–957.
88. U. Dydak, E. J. Ward, R. Ma, S. Snyder, S. E. Zauber, J. B. Murdoch, Z. Long and F. Rosenthal, Occupational Manganese Exposure Levels Correlate with Brain GABA Levels, *Proc. Intl. Soc. Mag. Reson. Med.*, 2014, **22**, 1895.
89. Z. Long, X. R. Li, J. Xu, R. A. Edden, W. P. Qin, L. L. Long, J. B. Murdoch, W. Zheng, Y. M. Jiang and U. Dydak, Thalamic GABA predicts fine motor performance in manganese-exposed smelter workers, *PLoS One*, 2014, **9**, e88220.
90. L. Long, Y. M. Jiang, X. R. Li, J. Xu, C. L. Yeh, L. L. Long, W. Zheng, J. B. Murdoch and U. Dydak, Increased Thalamic GABA and Decreased Glutamate-Glutamine in Chronic Manganese-exposed Metal Workers and Manganism Patients., *Proc. Intl. Soc. Mag. Reson. Med.*, 2014, **22**, 3777.
91. D. Le Bihan, J. F. Mangin, C. Poupon, C. A. Clark, S. Pappata, N. Molko and H. Chabriat, Diffusion tensor imaging: concepts and applications, *J. Magn. Reson. Imaging*, 2001, **13**, 534–546.
92. C. Beaulieu, The basis of anisotropic water diffusion in the nervous system – a technical review, *NMR Biomed.*, 2002, **15**, 435–455.
93. A. M. McKinney, R. W. Filice, M. Teksam, S. Casey, C. Truwit, H. B. Clark, C. Woon and H. Y. Liu, Diffusion abnormalities of the globi pallidi in manganese neurotoxicity, *Neuroradiology*, 2004, **46**, 291–295.
94. Y. Kim, K. S. Jeong, H. J. Song, J. J. Lee, J. H. Seo, G. C. Kim, H. J. Lee, H. J. Kim, J. H. Ahn, S. J. Park, S. H. Kim, Y. J. Kwon and Y. Chang, Altered white matter microstructural integrity revealed by voxel-wise analysis of diffusion tensor imaging in welders with manganese exposure, *Neurotoxicology*, 2011, **32**, 100–109.
95. A. Stepens, C. J. Stagg, A. Platkajis, M. H. Boudrias, H. Johansen-Berg and M. Donaghy, White matter abnormalities in methcathinone abusers with an extrapyramidal syndrome, *Brain*, 2010, **133**, 3676–3684.
96. P. Favrole, H. Chabriat, J. P. Guichard and F. Woimant, Clinical correlates of cerebral water diffusion in Wilson disease, *Neurology*, 2006, **66**, 384–389.

97. S. Ogawa, T. M. Lee, A. R. Kay and D. W. Tank, Brain magnetic resonance imaging with contrast dependent on blood oxygenation, *Proc. Natl. Acad. Sci. U. S. A.*, 1990, **87**, 9868–9872.
98. S. A. S. Huettel, A. W. Song and G. McCarthy, *Functional Magnetic Resonance Imaging*, Sinauer Associates, Inc., Sunderland, MA, USA, 2nd edn, 2009.
99. R. B. Buxton, *Introduction to functional magnetic resonance imaging: Principles and techniques*, Cambridge University Press, 2002.
100. Y. Chang, H. J. Song, J. J. Lee, J. H. Seo, J. H. Kim, H. J. Lee, H. J. Kim, Y. Kim, J. H. Ahn, S. J. Park, J. H. Kwon, K. S. Jeong and D. K. Jung, Neuroplastic changes within the brains of manganese-exposed welders: recruiting additional neural resources for successful motor performance, *Occup. Environ. Med.*, 2010, **67**, 809–815.
101. Y. Chang, J. J. Lee, J. H. Seo, H. J. Song, J. H. Kim, S. J. Bae, J. H. Ahn, S. J. Park, K. S. Jeong, Y. J. Kwon, S. H. Kim and Y. Kim, Altered working memory process in the manganese-exposed brain, *Neuroimage*, 2010, **53**, 1279–1285.
102. J. B. Bomanji, D. C. Costa and P. J. Ell, Clinical role of positron emission tomography in oncology, *Lancet Oncol.*, 2001, **2**, 157–164.
103. L. Mosconi, Brain glucose metabolism in the early and specific diagnosis of Alzheimer's disease. FDG-PET studies in MCI and AD, *Eur. J. Nucl. Med. Mol. Imaging*, 2005, **32**, 486–510.
104. R. E. Yee, I. Irwin, C. Milonas, D. B. Stout, S. C. Huang, K. Shoghi-Jadid, N. Satyamurthy, L. E. Delanney, D. M. Togasaki, K. F. Farahani, K. Delfani, A. M. Janson, M. E. Phelps, J. W. Langston and J. R. Barrio, Novel observations with FDOPA-PET imaging after early nigrostriatal damage, *Mov. Disord.*, 2001, **16**, 838–848.
105. S. Thobois, S. Guillouet and E. Broussolle, Contributions of PET and SPECT to the understanding of the pathophysiology of Parkinson's disease, *Neurophysiologie clinique/Clin. Neurophysiol.*, 2001, **31**, 321–340.
106. C. C. Huang, Parkinsonism induced by chronic manganese intoxication–an experience in Taiwan, *Chang Gung Med. J.*, 2007, **30**, 385–395.
107. C. C. Huang, Y. H. Weng, C. S. Lu, N. S. Chu and T. C. Yen, Dopamine transporter binding in chronic manganese intoxication, *J. Neurol.*, 2003, **250**, 1335–1339.
108. Y. Kim, J. M. Kim, J. W. Kim, C. I. Yoo, C. R. Lee, J. H. Lee, H. K. Kim, S. O. Yang, H. K. Chung, D. S. Lee and B. Jeon, Dopamine transporter density is decreased in parkinsonian patients with a history of manganese exposure: what does it mean?, *Mov. Disord.*, 2002, **17**, 568–575.
109. K. Tatsch and G. Poepperl, Nigrostriatal dopamine terminal imaging with dopamine transporter SPECT: an update, *J. Nucl. Med.*, 2013, **54**, 1331–1338.
110. H. Eriksson, J. Tedroff, K. A. Thuomas, S. M. Aquilonius, P. Hartvig, K. J. Fasth, P. Bjurling, B. Langstrom, K. G. Hedstrom and E. Heilbronn, Manganese induced brain lesions in Macaca fascicularis

as revealed by positron emission tomography and magnetic resonance imaging, *Arch. Toxicol.*, 1992, **66**, 403–407.

111. H. Shinotoh, B. J. Snow, K. A. Hewitt, B. D. Pate, D. Doudet, R. Nugent, D. P. Perl, W. Olanow and D. B. Calne, MRI and PET studies of manganese-intoxicated monkeys, *Neurology*, 1995, **45**, 1199–1204.
112. T. R. Guilarte, N. C. Burton, J. L. McGlothan, T. Verina, Y. Zhou, M. Alexander, L. Pham, M. Griswold, D. F. Wong, T. Syversen and J. S. Schneider, Impairment of nigrostriatal dopamine neurotransmission by manganese is mediated by pre-synaptic mechanism(s): implications to manganese-induced parkinsonism, *J. Neurochem.*, 2008, **107**, 1236–1247.
113. T. R. Guilarte, M. K. Chen, J. L. McGlothan, T. Verina, D. F. Wong, Y. Zhou, M. Alexander, C. A. Rohde, T. Syversen, E. Decamp, A. J. Koser, S. Fritz, H. Gonczi, D. W. Anderson and J. S. Schneider, Nigrostriatal dopamine system dysfunction and subtle motor deficits in manganese-exposed non-human primates, *Exp. Neurol.*, 2006, **202**, 381–390.
114. J. S. Schneider, E. Decamp, K. Clark, C. Bouquio, T. Syversen and T. R. Guilarte, Effects of chronic manganese exposure on working memory in non-human primates, *Brain Res.*, 2009, **1258**, 86–95.
115. M. K. Chen, J. S. Lee, J. L. McGlothan, E. Furukawa, R. J. Adams, M. Alexander, D. F. Wong and T. R. Guilarte, Acute manganese administration alters dopamine transporter levels in the non-human primate striatum, *Neurotoxicology*, 2006, **27**, 229–236.
116. E. C. Wolters, C. C. Huang, C. Clark, R. F. Peppard, J. Okada, N. S. Chu, M. J. Adam, T. J. Ruth, D. Li and D. B. Calne, Positron emission tomography in manganese intoxication, *Ann. Neurol.*, 1989, **26**, 647–651.
117. H. Shinotoh, B. J. Snow, N. S. Chu, C. C. Huang, C. S. Lu, C. Lee, H. Takahashi and D. B. Calne, Presynaptic and postsynaptic striatal dopaminergic function in patients with manganese intoxication: a positron emission tomography study, *Neurology*, 1997, **48**, 1053–1056.
118. Y. Kim, J. W. Kim, K. Ito, H. S. Lim, H. K. Cheong, J. Y. Kim, Y. C. Shin, K. S. Kim and Y. Moon, Idiopathic parkinsonism with superimposed manganese exposure: utility of positron emission tomography, *Neurotoxicology*, 1999, **20**, 249–252.
119. B. A. Racette, L. McGee-Minnich, S. M. Moerlein, J. W. Mink, T. O. Videen and J. S. Perlmutter, Welding-related parkinsonism: clinical features, treatment, and pathophysiology, *Neurology*, 2001, **56**, 8–13.
120. B. A. Racette, J. A. Antenor, L. McGee-Minnich, S. M. Moerlein, T. O. Videen, V. Kotagal and J. S. Perlmutter, [18F]FDOPA PET and clinical features in parkinsonism due to manganism, *Mov. Disord.*, 2005, **20**, 492–496.
121. S. R. Criswell, J. S. Perlmutter, J. S. Crippin, T. O. Videen, S. M. Moerlein, H. P. Flores, A. M. Birke and B. A. Racette, Reduced

uptake of FDOPA PET in end-stage liver disease with elevated manganese levels, *Arch. Neurol.*, 2012, **69**, 394–397.
122. K. Sikk, P. Taba, S. Haldre, J. Bergquist, D. Nyholm, H. Askmark, T. Danfors, J. Sorensen, L. Thurfjell, R. Raininko, R. Eriksson, R. Flink, C. Farnstrand and S. M. Aquilonius, Clinical, neuroimaging and neurophysiological features in addicts with manganese-ephedrone exposure, *Acta Neurol. Scand.*, 2010, **121**, 237–243.
123. S. R. Criswell, J. S. Perlmutter, T. O. Videen, S. M. Moerlein, H. P. Flores, A. M. Birke and B. A. Racette, Reduced uptake of [(1)(8)F]FDOPA PET in asymptomatic welders with occupational manganese exposure, *Neurology*, 2011, **76**, 1296–1301.
124. K. P. Bhatia and C. D. Marsden, The behavioural and motor consequences of focal lesions of the basal ganglia in man, *Brain*, 1994, **117**(Pt 4), 859–876.
125. J. Rodier, Manganese poisoning in Moroccan miners, *Br. J. Ind. Med.*, 1955, **12**, 21–35.
126. R. M. Park, R. M. Bowler and H. A. Roels, Exposure-response relationship and risk assessment for cognitive deficits in early welding-induced manganism, *J. Occup. Environ. Med./Am. Coll. Occup. Environ. Med.*, 2009, **51**, 1125–1136.
127. R. M. Bowler, S. Nakagawa, M. Drezgic, H. A. Roels, R. M. Park, E. Diamond, D. Mergler, M. Bouchard, R. P. Bowler and W. Koller, Sequelae of fume exposure in confined space welding: a neurological and neuropsychological case series, *Neurotoxicology*, 2007, **28**, 298–311.
128. T. R. Guilarte, Manganese and Parkinson's disease: a critical review and new findings, *Environ. Health Perspect.*, 2010, **118**, 1071–1080.
129. B. S. Twining, S. B. Baines, N. S. Fisher, J. Maser, S. Vogt, C. Jacobsen, A. Tovar-Sanchez and S. A. Sanudo-Wilhelmy, Quantifying trace elements in individual aquatic protist cells with a synchrotron X-ray fluorescence microprobe, *Anal. Chem.*, 2003, **75**, 3806–3816.
130. M. D. de Jonge, C. Holzner, S. B. Baines, B. S. Twining, K. Ignatyev, J. Diaz, D. L. Howard, D. Legnini, A. Miceli, I. McNulty, C. J. Jacobsen and S. Vogt, Quantitative 3D elemental microtomography of Cyclotella meneghiniana at 400-nm resolution, *Proc. Natl. Acad. Sci. U. S. A.*, 2010, **107**, 15676–15680.
131. A. Carmona, G. Deves, S. Roudeau, P. Cloetens, S. Bohic and R. Ortega, Manganese accumulates within golgi apparatus in dopaminergic cells as revealed by synchrotron X-ray fluorescence nanoimaging, *ACS Chem. Neurosci.*, 2010, **1**, 194–203.
132. R. Ortega, G. Deves and A. Carmona, Bio-metals imaging and speciation in cells using proton and synchrotron radiation X-ray microspectroscopy, *J. R .Soc., Interface*, 2009, **6**(Suppl 5), S649–658.
133. A. Daoust, E. L. Barbier and S. Bohic, Manganese enhanced MRI in rat hippocampus: a correlative study with synchrotron X-ray microprobe, *Neuroimage*, 2013, **64**, 10–18.

134. G. Robison, T. Zakharova, S. Fu, W. Jiang, R. Fulper, R. Barrea, W. Zheng and Y. Pushkar, X-ray fluorescence imaging of the hippocampal formation after manganese exposure, *Metallomics*, 2013, **5**, 1554–1565.
135. G. Robison, T. Zakharova, S. Fu, W. Jiang, R. Fulper, R. Barrea, M. A. Marcus, W. Zheng and Y. Pushkar, X-ray fluorescence imaging: a new tool for studying manganese neurotoxicity, *PLoS One*, 2012, **7**, e48899.
136. A. Carmona, S. Roudeau, L. Perrin, G. Veronesi and R. Ortega, Environmental manganese compounds accumulate as Mn(ii) within the Golgi apparatus of dopamine cells: relationship between speciation, subcellular distribution, and cytotoxicity, *Metallomics*, 2014, **6**, 822–832.
137. Y. Kim, Neuroimaging in manganism, *Neurotoxicology*, 2006, **27**, 369–372.
138. V. A. Fitsanakis, N. Zhang, M. J. Avison, J. C. Gore, J. L. Aschner and M. Aschner, The use of magnetic resonance imaging (MRI) in the study of manganese neurotoxicity, *Neurotoxicology*, 2006, **27**, 798–806.
139. M. Aschner, T. R. Guilarte, J. S. Schneider and W. Zheng, Manganese: recent advances in understanding its transport and neurotoxicity, *Toxicol. Appl. Pharmacol.*, 2007, **221**, 131–147.